Nanoreinforcement strategies for enhancing biodegradable composites in biochemical applications within agriwaste valorisation

Imane Ziani, Abdelqader El Guerraf, Nour Eddine Bentouhami, Mohamed Brahmi, Hamza Bouakline, Ali El Bachiri, Marie-Laure Fauconnier, Sabah Ansar, Farooq Sher

PII: S1878-8181(24)00207-X

DOI: https://doi.org/10.1016/j.bcab.2024.103223

Reference: BCAB 103223

To appear in: *Biocatalysis and Agricultural Biotechnology*

Received Date: 5 March 2024

Revised Date: 26 April 2024

Accepted Date: 10 May 2024

Please cite this article as: Ziani, I., El Guerraf, A., Bentouhami, N.E., Brahmi, M., Bouakline, H., El Bachiri, A., Fauconnier, M.-L., Ansar, S., Sher, F., Nanoreinforcement strategies for enhancing biodegradable composites in biochemical applications within agriwaste valorisation, *Biocatalysis and Agricultural Biotechnology*, https://doi.org/10.1016/j.bcab.2024.103223.

Nanoreinforcement strategies for enhancing biodegradable composites in biochemical applications within agriwaste valorisation

Imane Ziani[1,2,*], Abdelqader El Guerraf [2,3,4], Nour Eddine Bentouhami[5], Mohamed Brahmi[1], Hamza Bouakline[1], Ali El Bachiri[1], Marie-Laure Fauconnier[6], Sabah Ansar[7], Farooq Sher[8,*]

[1]*Physical Chemistry of Natural Substances and Process Research Team, Laboratory of Applied Chemistry and Environment, Department of Chemistry, Faculty of Sciences, Mohammed First University, Oujda 60000, Morocco*

[2]*International Society of Engineering Science and Technology, Nottingham, United Kingdom*

[3]*J. Heyrovsky Institute of Physical Chemistry, Dolejškova 2155, Libeň, 18200 Praha 8, Czechia*

[4]*Laboratory of Applied Chemistry and Environment, Faculty of Science and Techniques, University Hassan First, BP. 577, Settat 26000, Morocco*

[5]*Bio-Resources, Biotechnology, Ethno-Pharmacology and Health. Research Team, Faculty of Sciences, Biology Department, Mohammed First University, 60000 Oujda, Morocco*

[6]*Laboratory of Chemistry of Natural Molecules, Gembloux Agro-Bio Tech, University of Liège, Liège, Belgium*

[7]*Department of Clinical Laboratory Sciences, College of Applied Medical Sciences, King Saud University, P.O. Box 10219, Riyadh, 11433, Saudi Arabia*

[8]*Department of Engineering, School of Science and Technology, Nottingham Trent University, Nottingham NG11 8NS, United Kingdom*

***Corresponding authors:**

Dr. F. Sher
Assistant Professor
Department of Engineering, School of Science and Technology
Nottingham Trent University
Nottingham
NG11 8NS
UK
E-mail address: Farooq.Sher@ntu.ac.uk (F. Sher), imane.ziani95@outlook.com (I. Ziani)

Tel.: +44 (0) 115 84 86679

Abstract

Exploring secondary outputs, specifically leftover materials from steam distillation of *Rosmarinus tournefortii* de Noé, as agents for reducing metals introduces a novel approach to eco-friendly nanomaterial production. This concept aligns with the creation of environmentally conscious nanoparticles, showcasing potential across various fields, notably biomedicine. The paper seamlessly fits into this context. By utilizing *R. tournefortii* de Noé, successful synthesis of silver nanoparticles (AgNPs) was achieved, yielding nanoscale variations influenced by the plant's by-products. Beyond structural aspects, investigating biomedical applications, focusing on antioxidant and antimicrobial properties. Consistently observing ~94.9–97.3% scavenging inhibition in water residues at different concentrations and enhanced antimicrobial efficacy against Gram-negative and Gram-positive bacteria and *Rhodotorula glutinis* yeast due to these residues. Moreover, a thorough examination using density functional theory unveiled a robust interaction between silver clusters and specific biomolecules found within the residues, namely homoplantaginin, protocatechuic acid-glycoside, caffeic, and rosmarinic acids (ranging from 130.62 to 357.05 kcal/mol). These compounds notably enhance the reducing efficacy of Ag+ ions and contribute to the enduring stability of AgNPs (ζ values: -22.8 mV and -17.2 mV). Furthermore, the study recognizes challenges in finding alternative surface modification agents and explores the intricate toxicity mechanisms of silver nanoparticles, emphasizing their interactions with inflammation. Introducing promising nanomedicine approaches involving rosmarinic acid nanoparticles for inflammatory bowel disease and rheumatoid arthritis, highlighting the potential of rosemary by-products derived compounds in innovative therapeutic interventions for diverse inflammatory conditions.

Keywords: *Rosmarinus tournefortii* de Noé; Sustainability; Bioconversion; Bio-based materials; nano reinforcement; Antioxidant; biodegradable and DFT optimization.

1. Introduction

Nanotechnology stands as one of the most rapidly advancing domains in the realm of science and technology on a global scale. In this vein, the fabrication of metal nanoparticles constitutes an actively investigated area within nanotechnology, exhibiting exponential advancements across biomedical applications, nutritional sciences, and energy applications (Mittal et al., 2013). The challenge of achieving a biogenetic synthesis of uniformly sized nanoparticles with distinct shapes remains at the forefront of biomaterials science. This achievement has also rendered substantial advantages within the pharmaceutical sector, particularly in the struggle against an array of bacterial and viral infections (Huh and Kwon, 2011). A broad spectrum of techniques encompassing physical, chemical, biological, and hybrid methodologies is currently employed to engineer nanoparticles of varying properties. Nonetheless, physical and chemical synthesis methods are frequently hindered by elevated production expenses, ecological pollution, and biological hazards (Bereza-Malcolm et al., 2015). Consequently, the biological approach emerges as an alternative to traditional chemical and physical methods, serving as an eco-friendly avenue for nanoparticle production. Moreover, this approach obviates the necessity for costly, perilous, and toxic substances (Naghdi et al., 2022).

Ongoing investigations into the bio-production of non-metallic substances through botanical extracts have unveiled a fresh avenue, offering swift and benign techniques within the redox reaction for the creation of environmentally conscious nanoparticles. A multitude of scholars have documented the biogenic synthesis of metal nanoparticles via plant leaf extracts, spotlighting their potential uses. This propensity is ascribed to the presence of secondary metabolites, encompassing phenolic acids, flavonoids, alkaloids, and terpenoids, which primarily contribute to the conversion of ions into substantial metal nanoparticles (Pisoschi et al., 2022). Several antecedent studies have underscored the proficiency of biosynthesized

nanoparticles in regulating oxidative stress, genotoxicity, and changes associated with apoptosis (Zhang et al., 2018). Furthermore, nanoparticles boast an extensive array of applications within the domains of agriculture and plant sciences. For instance, through the utilization of bioprocessing technology, nanoparticles can transform agricultural and food residues into energy (Tariq et al., 2023) and valuable by-products (Usmani et al., 2022).

Moreover, researchers have extensively explored the utilization of lignocellulosic biomass for synthesizing metallic nanoparticles, elucidating its manifold applications and advantages. Chen et al. (Chen et al., 2023) emphasize green synthesis methods using biomass components like cellulose, hemicellulose, and lignin, resulting in nanoparticles with unique properties applicable in catalysis, sensing, and biomedicine. For instance, cellulose-derived nanoparticles exhibit high catalytic activity, with conversion rates exceeding 90% in chemical reactions, while hemicellulose-derived ones demonstrate exceptional sensing capabilities, detecting pollutants at concentrations as low as 1 ppb (Chen et al., 2023). Lignin-derived nanoparticles show promising antimicrobial properties, with inhibition rates of up to 95% against bacteria, underscoring sustainability (Chen et al., 2023). Conversely, Sankaran et al. (Sankaran et al., 2021) focus on enhancing bioenergy production through biomass-to-nanoparticle conversion. They highlight the use of magnetite nanoparticles (MNPs) alongside alkaline pretreatment on rice straw, resulting in a significant increase in biogas and methane yield by 100% and 129% respectively (Sankaran et al., 2021). Additionally, incorporating nanoparticles into acid-functionalized magnetic nanoparticles boosts sugar production by 46% (Sankaran et al., 2021). Both studies underscore the value of biomass for nanoparticle synthesis, addressing various fields and offering sustainable solutions.

Despite the widespread use of plant extracts for nanoparticle synthesis, one of the most recent and promising methods, based on the natural "bio-laboratory," is the use of biodegradable wastes generated by the agricultural and food industries. Moreover, these waste materials are abundant, cost-effective, and readily available, obviating the need for elaborate pre-processing procedures. Various experiments were conducted to synthesize nanoparticles using different waste sources. In this context, zinc oxide nanoparticles were produced employing waste from Phoenix dactylifera as a bio-reductant for efficient dye degradation and antibacterial effectiveness in wastewater treatment (Rambabu et al., 2021). PVP-coated silver nanoparticles (PVP-AgNPs) were employed in municipal solid waste composting (Gitipour et al., 2013). Additionally, the Fenton process employed copper nanoparticles derived from printed circuit boards to degrade mining surfactant (Martins et al., 2021). Secondary metabolites, which are the main metal-reducing agents in the "green" synthesis of nanoparticles, are found naturally in waste from the essential oil industry. Raw materials with a low essential oil content generate a lot of waste. Although distilleries generally dispose of their residues, these common practices can disrupt the ecological balance of the site and result in the loss of valuable biologically active substances present in the waste (Da Silva et al., 2016).

Amidst the diverse tapestry of rosemary species, *Rosmarinus officinalis* L. stands revered for its therapeutic prowess and the generous yield of its essential oils. However, a notable void exists in the expansive landscape an absence of comprehensive exploration into the species *Rosmarinus tournefortii* de Noé. While *R. officinalis* L., has received considerable attention, the intricacies of *Rosmarinus tournefortii* de Noé have been largely overlooked. This study aims to fill this void by uncovering the untapped potential of *Rosmarinus tournefortii* de Noé, particularly in utilizing its waste by-products for nanoparticle synthesis. Specifically, the focus is on utilizing water and solid by-products as reduction agents for Ag, Zn, and Cu metal ions.

The synthesis process was meticulously characterized using advanced techniques to provide comprehensive insights into the resulting materials. Additionally, specialized analyses were conducted to evaluate the efficacy of biomolecules within each by-product, with a comparative analysis between water and solid by-products to understand their roles in nanoparticle synthesis and their effectiveness as reduction agents.

Moreover, the study delves into the potential biological applications of the synthesized nanoparticles, particularly their antioxidant and antimicrobial properties, suggesting promising avenues in medicine and materials science. However, challenges and unexplored territories remain. The exploration of alternative complexation agents for nanoparticle surface modification is identified as a growing research area to enhance nanoparticle stability and functionality. Additionally, the study underscores the promising potential for health-enhancing applications in drug delivery and medical imaging. Overall, this study showcases the ability to repurpose industrial by-products for eco-friendly nanoparticle synthesis, showcasing accomplishments while highlighting avenues for future investigation. This multidisciplinary approach positions by-product-derived nanoparticle synthesis as a key player in sustainable nanotechnology and its myriad applications.

2. Materials and methods

2.1. Plant material extraction

The untamed *Rosmarinus tournefortii* de Noé plant's fresh leaves were harvested amidst its flowering phase on March 13, 2020, within the Megrez forest region of eastern Morocco, located at coordinates 34° 43′ 52.6″ N 2° 04′ 21.5″ W (Ziani et al., 2023). The plant's identification was confirmed by Tahri Tahar, the director of the Forest Management Studies Service of Oriental, Morocco. Voucher specimens were deposited at the Physical Chemistry of Natural Substances and Process Laboratory, Faculty of Sciences, Mohammed First University,

Oujda, Morocco. These leaves, once dried, underwent steam distillation on a semi-pilot scale to extract the pertinent essential oil. The liquid residue produced during steam distillation was separated from the solid residue through filtration using a 90 mm Whatman (GF/A) filter and subsequently concentrated utilizing a rotary evaporator. In the case of the solid residue, it was pulverized and air-dried over a period of approximately 15 days. Following this, the residue was subjected to de-ionized water extraction for an hour. The resultant extracts from the two categories of rosemary by-products, namely the liquid and solid residues, were securely stored in amber glass vials and maintained at a refrigerated temperature of 4 °C until subjected to analysis.

2.2. Biosynthesis of silver, zinc and copper nanoparticles

In the process of green synthesizing Ag, Zn, and Cu-NPs, the well-established protocol by Raut et al. (Raut et al., 2014) was adapted with minor adjustments. The initial step involved dissolving 2.5 g of liquid and solid residue extracts in 50 mL of de-ionized water to formulate the aqueous extracts. Silver nitrate, zinc nitrate, and copper nitrate served as the precursor materials for Ag, Zn, and Cu nanoparticles. The prepared extract was then introduced to 0.1 M solutions of $AgNO_3$, $ZnNO_3$, and $CuNO_3$, maintaining a ratio of 1:2 (v/v). The solution mixture was agitated at 70 °C for 3 hours. After the nanoparticle synthesis was finalized, centrifugation was employed to isolate Ag, Zn, and Cu-NPs. The supernatant was separated post-centrifugation, and the resulting precipitates underwent triple washing using de-ionized water, followed by drying at 60 °C for two days (**Fig. 1**).

2.3. Characterization of biosynthesized nanoparticles

To confirm the generation of nanoparticles, a Shimadzu UV 1650-PC UV-visible spectrophotometer was utilized. The measurement of absorbance was carried out within the range of 300–800 nm (Lv et al., 2021). Attenuated Total Reflectance-Fourier Transform

Infrared (ATR-FTIR) analysis was executed employing a Jasco 4700-FTIR spectrometer from Shimadzu, Japan. This was done to compare the characteristics of the dried plant material with those of the synthesized nanoparticles, aiming to decipher the role of reducing agents in metallic ion reduction. The absorption spectra were captured over a wavelength range of 400 to 4000 cm^{-1} (Borah et al., 2021). Microstructural scrutiny of the developed charged nanoparticles was performed using a JEOL-JSM7001F instrument and field-emission scanning electron microscopy (FE-SEM). The SEM filament operated at various currents and a voltage of 5 kV at different magnifications, while the fixed working distance was maintained at 6 mm (representing the unchanging separation between the sample and the objective lens). Elemental composition was determined through X-ray energy dispersive spectroscopy (EDS). The mean diameter and distribution of the nanoparticles were measured using a laser granulometer, specifically the Anton Paar Litesizer 500 (de Souza Niero et al., 2023). These measurements were executed at room temperature within a liquid cell containing a dispersant with a refractive index of 1.33. Zeta potential was determined via electrophoresis and the application of the Smoluchowski equation to analyze particle mobility. XRD patterns of all nanoparticle samples were captured using a Shimadzu XRD-6000 diffractometer and a Cu K ($\lambda = 0.154$ nm) radiation source. Data collection occurred at a scanning speed of 0.02°/s within a diffraction angle span of 10° to 80°. The crystallite sizes of the nanoparticles were deduced utilizing the Scherrer formula (**Eq. (1)**) (El Guerraf et al., 2023), with the average diameter of silver crystals (D) being calculated based on the (111) plane.

$$D = \frac{K\lambda}{\beta COS\theta} \quad \textbf{(1)}$$

2.4. Matrix of rosemary by-products

In the evaluation of rosemary by-products, a High-Performance Liquid Chromatography (HPLC) System, furnished with a 2998 Photodiode Array Detector and a reversed-phase C18 column (5, 250 × 4.6 mm), was utilized. Following the procedure outlined by Liu et al. (Liu et

al., 2011), extracts with a concentration of 5 mg/mL were introduced into the column, flowing at a rate of 0.8 mL/min, utilizing a gradient mixture of binary solvents. To separate phenolic compounds, a mobile phase consisting of two constituents was employed: mobile phase A (acetonitrile with 0.1% formic acid) and mobile phase B (water with 0.1% formic acid). The gradient pattern followed this sequence: starting at 60% B at 0 minutes, transitioning to 50% B at 2 minutes, maintaining 50% B at 10 minutes, decreasing to 30% B at 15 minutes, maintaining 30% B at 25 minutes, and returning to 60% B at 32 minutes. To identify specific phenolic components, their retention time and maximum wavelength were assessed and compared against established standards and available literature data.

2.5. DPPH radical scavenging assay

The 2,2-diphenyl-1-picrylhydrazyl (DPPH) assay was carried out with a slight alteration derived from our previously outlined procedure (El Guerraf et al., 2023). This assay is commonly employed to evaluate the antioxidant potential of environmentally produced nanoparticles. In a concise summary, varying concentrations (0.1, 0.5, 1, 1.5 and 2 mg) of the nanoparticles were mixed with 2500 µL of DPPH solution in methanol (0.04 mg/mL). After being left in the dark for 60 minutes, the absorbance at 517 nm was gauged via a UV-vis spectrophotometer. The scavenging inhibition (%) was determined using the subsequent formula, depicted by **Eq. (2)**, in which A0 symbolizes the absorbance of the control, and AC signifies the absorbance of the tested samples.

$$DPPH\ Inhibition\ (\%) = \frac{A0-AC}{A0} \times 100 \quad \textbf{(2)}$$

2.6. Anti-microbial properties

Following prior investigations (Abdollahzadeh et al., 2021), the agar diffusion method was employed to assess the antibacterial properties of nanoparticles synthesized from rosemary by-products on solid surfaces. The in vitro antibacterial performance was evaluated against distinct

microorganisms, namely *Listeria innocua* ATCC 33090 (gram-positive bacteria), *Escherichia coli* ATCC 25922 (gram-negative bacteria), along with *Rhodotorula glutinis* (yeast) and *Geotrichum sp*. (mold). For both microbial types, the strains were adjusted to a 0.5 McFarland standard, equivalent to 10^6 CFU/mL and 10^6 spores/mL, correspondingly (Mahdi et al., 2022). Afterwards, these cultures were additionally thinned using Mueller-Hinton broth for bacteria, yeast, and mould, and sterile physiological water for both, before being introduced onto the surface of petri dishes. In this approach, wells (6 mm) were generated in Mueller-Hinton agar (MHA) previously inoculated with the target bacteria or fungus. These wells were subsequently loaded with 10 µL of samples (10 mg/mL). Incubation of the agar plates facilitated bacterial and fungal growth, conducted at 37°C for 18 hours and 25°C for 48 hours respectively. The antimicrobial efficacy was evaluated by measuring the size of the inhibition zone within the agar medium. To ensure robustness, each assay was carried out in triplicate.

2.7. Computational study

Initially, the major compounds (namely, caffeic acid, homoplantaginin, protocatechuic acid-glycoside, rosmarinic acid, epicatechin, and gallocatechin) extracted from *Rosmarinus tournefortii* de Noé by-products were optimized at the ground state using the GAUSSIAN 09 quantum chemistry simulation software (Kaushik et al., 2022). Subsequently, each individual molecule was optimized in conjunction with a silver cluster by placing it in close proximity to reactive sites that were identified through analyses of molecular electrostatic potential (MEP). To reduce computational costs, representative models of silver nanoparticles (AgNPs), consisting of a single silver atom (Ag_1) and three silver atoms (Ag_3) clusters, were utilized. The interaction energies between the AgNPs models and the target molecules were estimated using **Eq. (3)** (Kaushik et al., 2022).

$$\Delta I = E_{Ag\text{-}compound} - (E_{Ag} + E_{compound}) \quad \textbf{(3)}$$

Where $E_{Ag\text{-}compound}$, E_{Ag}, and $E_{compound}$ represent the energies associated with the interaction between AgNPs and the target molecule, AgNPs themselves, and the target compound, respectively. The optimization through DFT was performed using the B3LYP hybrid functional at the Lee-Yang-Parr calculation level. The organic compounds underwent treatment with the 6-311G(d,p) basis set, whereas the Ag atoms were characterized using the LanL2DZ basis set. Conventional convergence criteria were applied, and visualization of the molecular structure was facilitated using the GaussView 5.0 molecular editor.

3. Results and discussion

3.1. Optical absorption and crystalline structure analysis

UV-vis spectroscopy is a highly effective method for analyzing the optical response of metal nanoparticles, particularly sensitive to their formation due to the pronounced surface plasmon resonances (SPRs) they exhibit (Kelly et al., 2003). In this study, the UV-vis absorption spectra of colloidal nanoparticles produced from the two types of rosemary residues were examined. The spectral data demonstrated distinctive surface plasmon (SP) bands associated with AgNPs, showing variations in their "λmax" and intensity of the SP band. This distinction underscores the evident impact of the compound's characteristics on these particular parameters. In contrast, when Zn and Cu were employed for nanoparticle synthesis, the SP band intensity spectra remained unchanged, indicating the unsuccessful development of ZnNPs and CuNPs. The consistent surface plasmon (SP) band intensity spectra observed during the utilization of Zn and Cu for nanoparticle synthesis suggest the unsuccessful development of ZnNPs and CuNPs, potentially due to various factors. Inadequate synthesis conditions, such as suboptimal temperature, pH, or reaction time, could have led to the formation of nanoparticles with properties deviating from the desired plasmonic characteristics (Kim et al., 2024).

Additionally, the propensity of Zn and Cu nanoparticles to oxidize in air or aqueous environments may have resulted in the formation of oxide layers on the nanoparticle surface, affecting their plasmonic properties (Jahan et al., 2021). Agglomeration or aggregation of nanoparticles during synthesis or post-synthesis treatments could have altered the interactions between nanoparticles, impacting the observed SP band intensities (Pryshchepa et al., 2020). Furthermore, surface contamination with impurities or residues from the synthesis process might have interfered with the plasmonic properties of ZnNPs and CuNPs. The absence of appropriate surface ligands or stabilizing agents during synthesis could have led to unstable nanoparticles with modified plasmonic behavior (Kim et al., 2023). These factors collectively contribute to the challenges in achieving the successful development of ZnNPs and CuNPs with the desired plasmonic properties.

The spectra were captured when the colloidal sample's colour and absorption strength remained constant. **Fig. 2(a, b)** illustrates that each residue used exhibits a single, distinct SPR position in the 300–500 nm range. Additionally, no SPRs were seen at wavelengths greater than 500 nm, suggesting that the majority of the AgNPs produced have small sizes and comparable shapes. This observation also provides early clues about colloidal AgNPs' size and size distribution. Comparing the plasmon band positions of the two different residues, the solid residue revealed higher wavelengths (372 nm) than the water residue (368 nm), demonstrating a reduction in AgNPs particle size. Similar to this, several earlier studies from the *Rosmarinus officinalis* L. plant species have also noted the absorption spectrum between 350 and 500 nm brought on by AgNPs' surface plasmon resonance (Ghaedi et al., 2015; Noukelag et al., 2021).

X-ray diffraction (XRD) and Fourier-transform infrared spectroscopy (FTIR) were conducted to gain information on the one hand about the size, lattice, and structure of nanoparticles, and

on the other hand, about any potential bioactive compounds present in *Rosmarinus tournefortii* de Noé and that can possibly act as reducing/stabilizing agent. For a better comparison, the spectroscopic analysis was achieved in the case of Zn, Cu, and Ag biosynthesized in the presence of the two types of rosemary by-products; solid and water residues. Firstly, by analysing the XRD pattern obtained for the tested by-products, it is clear the amorphous nature of both SR and WR (**Fig. 2(c, d)**). When using Zn or Cu, the XRD spectra remain unchanged suggesting the unsuccessful elaboration of ZnNPs and CuNPs. The diffractograms resulted for silver nanoparticles were totally different as they showed four well-resolved peaks at 2θ angles of 38.27°, 44.38°, 64.62° and 77.52° for SR, and 38.15°, 44.32°, 64.55°, and 77.45° in the case of WR. These prominent peaks arise from the (111), (200), (220), and (311) Bragg reflections of face-centred cubic (fcc) structures of AgNPs (JCPDS 04-0783). Further, the average crystallite size (d) of AgNPs was estimated using the Debye-Scherrer equation, $d = K\lambda/\beta\cos\theta$ where K is the shape factor (between 0.9 and 1.1), λ is the incident X-ray wavelength of Cu Kα radiation (1.542 Å), β is the full width at half maximum in radians of the (111) line, and θ is the Bragg diffraction angle. The average AgNPs sizes were found to be 17.98 and 18.49 nm for SR@AgNPs and WR@AgNPs composites, respectively. The obtained results are more interesting than those of Das et al. (Das and Velusamy, 2013) and Ghaedi et al. (Ghaedi et al., 2015) where it was reported that the mean AgNPs particle size ranged from 31.79 to 33 nm for the plant genus *Rosmarinus officinalis* L. respectively.

On the other hand, FTIR characterization for all samples resulted in the spectra presented in (**Fig. 2(e, f)**). For both SR and WR, several typical bands were observed that describe functional groups associated with various biological macromolecules in the Rosemary leaf extracts. The peak with relatively high intensity at 1020 cm^{-1} is assigned to C-O-C stretching vibration or alcohols/phenols (Farshchi et al., 2018). The bands at around 1152 and 1256 cm^{-1} arise from

C–O stretching and represent the presence of polyphenols and the one that appears at 1391 cm^{-1} corresponds to C–O–C stretching modes of vibration. The signal at 1514 cm^{-1} demonstrates also the presence of phenolic compounds from the extract which is related to the stretching of the aromatic rings (Farshchi et al., 2018). The peak detected at approximately 1587 cm^{-1} may result from the vibration of C=C groups, while the one near 1713 cm^{-1} is associated with C=O groups from carboxylic acids (Piñeros-Hernandez et al., 2017). The stretching vibration of C–H is justified by the peak appearing at 2931 cm^{-1}. Finally, the broad absorption band at a wavenumber between 3020-3620 cm^{-1} is linked to O–H stretching (Piñeros-Hernandez et al., 2017).

After the bio-synthesis of AgNPs, the spectrum remains practically unchanged demonstrating that the metal nanoparticles did not alter the structure of the rosemary plant in a significant way. It should be noted, however, that some IR bands were shifted to lower frequencies after the interaction of the residues with Ag. Based on the ATR-FTIR results and previously reported papers for *Rosmarinus officinalis* L. species (Rabiee et al., 2020), the mechanism of reducing silver ions to metallic silver can be discussed. In a simple way, numerous bioactive compounds from *Rosmarinus tournefortii* de Noé will surround Ag^{+} producing a coating. The latter receive electrons from these phytochemical constituents resulting in the reduction of silver cation and avoiding the agglomeration of the particles. Most likely, the carbonyl groups from the bioactive compounds are responsible for the reduction process and can act as a stabilizer and bio-capping agents of the AgNPs. In summary, the spectroscopic analyses have demonstrated the successful green synthesis of AgNPs using both *Rosmarinus tournefortii* de Noé solid and water residues. Apart from Zn and Cu, no promising results were obtained, which may be related to the absence of sufficient reducing agents or suitable biomolecules to facilitate the reduction of metal ions, thus hindering NPs formation.

The limitations in ATR-FTIR analysis, despite comparing plant extract with synthesized CuNPs or ZnNPs, stem from challenges inherent in the nanoparticle synthesis process, as evidenced by prior UV-vis and DRX analyses. Incomplete reduction of metal ions during synthesis may hinder the formation of well-defined nanoparticles with distinct chemical characteristics (Adra et al., 2024). Moreover, issues like nanoparticle aggregation or precipitation, due to inadequate stabilization or unfavorable reaction conditions, can obscure changes in the ATR-FTIR spectra. These aggregated nanoparticles may exhibit broad or overlapping peaks, making it challenging to discern specific features. Additionally, the sensitivity of ATR-FTIR may not be sufficient to detect subtle changes in chemical composition or surface functional groups, particularly with low nanoparticle concentration or minimal changes (Lee and Chae, 2021). Background signals or noise in the spectra could further complicate the analysis. Weak or transient interactions between plant extract components and Cu or Zn ions may result in subtle or undetectable changes in FTIR spectra, possibly due to the nature of binding sites on the plant extract molecules (Jędrzejczyk et al., 2023). Together, these factors contribute to the limited changes observed in ATR-FTIR analysis following unsuccessful nanoparticle synthesis. As the mechanism of interaction remains always hard to fully understand, further optimization of the experimental conditions may be necessary in future studies. It is essential to highlight that this study primarily concentrated on the synthesis of nanoparticles from *Rosmarinus tournefortii* de Noé, a species not previously investigated for this purpose, suggesting avenues for future exploration.

3.2. Hydrodynamic size and surface analysis

The enduring stability of colloidal silver nanoparticles was observed through spectroscopic monitoring using the zeta potential technique. This method, commonly employed for managing the stability of colloidal metal nanoparticles, gauges alterations in surface charge. Metal nanoparticles possessing a notably positive or negative zeta potential exhibit mutual repulsion,

383 preventing them from aggregating. Conversely, particles with low absolute zeta potential
384 values tend to aggregate and coalesce due to the absence of repulsive forces that hinder such
385 accumulation (Rao et al., 2021). Zeta potential (ζ) results for the two types of *Rosmarinus*
386 *tournefortii* de Noé steam distillation by-products; solid residues and water have ζ values of -
387 13.3 and -11.4 mV, while the freshly prepared colloidal AgNPs have ζ values of -22.8 and -
388 17.2 mV, respectively. The results obtained showed a strong negative value for AgNPs, clearly
389 suggesting the stability of nanoparticles. Moreover, the stability and colloidal behaviour of the
390 nanoparticles were explored as shown in **Fig. 3(a, b)**, yielding insightful findings. Notably, a
391 single peak position was observed on the distribution graph for SR@AgNPs, indicating that
392 the nanoparticles in this residue exhibited a uniform size of approximately 92.3 nm and shared
393 a similar surface charge. Such uniformity is characteristic of a monodisperse (narrowly
394 distributed) sample, which holds significant appeal for numerous applications. Additionally,
395 intriguingly, WR@AgNPs displayed two distinct peaks in the nanoparticle size distribution
396 (62.2 and 111.64 nm). Each peak represented a group of particles with comparable sizes. This
397 bimodal distribution suggested the existence of two separate populations of nanoparticles in
398 the sample. Possible explanations for this phenomenon could include the aggregation or
399 agglomeration of nanoparticles, resulting in larger particles that contribute to the second peak
400 in the size distribution. Furthermore, the presence of various morphologies or crystalline
401 structures among the nanoparticles might also contribute to the bimodal size distribution. For
402 instance, certain metal nanoparticles can exhibit different shapes, such as spherical and rod-
403 shaped, leading to diverse size populations (Yaraki et al., 2022).
404
405 Additional support for the successful production of AgNPs was uncovered through
406 morphological examinations and elemental analysis. As illustrated in **Fig. 3(c, d)**, the obtained
407 nanoparticles exhibited distinct shapes. The two types of by-products displayed predominantly

spherical morphology in their nanoparticles, each exhibiting varying diameters within the nanoscale range. Because of their diminutive size, extensive surface activity, and considerable specific surface area, the nanoparticles had a proclivity to readily form aggregates. The effectiveness of synthesizing AgNPs using *Rosmarinus tournefortii* de Noé solid and water residues was further confirmed by analyzing the chemical composition based on the EDX spectrum (**Fig. 3(e, f)**). The optical absorption band of the EDX peak in the 3-4 keV range is characteristic of metallic silver nanocrystallites' absorption (Kotakadi et al., 2014). The EDX spectrum of the synthesized silver nanoparticles (**Fig. 3(e, f)**) clearly showed the absence of elemental nitrogen peaks and the presence of elemental silver metal, along with C and O, which are associated with the phenolic compounds of the residues and the formation of Ag NPs. The distinct signal peak of silver provided strong evidence of the successful reduction of silver nitrate to silver nanoparticles. Our findings align with earlier studies on AgNPs produced from the *Rosmarinus officinalis* L. plant species (Das and Velusamy, 2013; Ghaedi et al., 2015). Those studies also noted the presence of uniformly sized, spherical silver nanoparticles in the nanoscale range.

3.3. Matrix responsible for metal ion reduction

Many active plant chemicals with therapeutic or dietary benefits have been used to create nanomaterials. Among these, flavonoids and phenolic acids have received a great deal of attention because of their potential uses in nano-medicine. To better understand the nature of the molecules responsible for stabilization and reduction in the synthesis of metal NPs, HPLC-DAD analysis was carried out. Through comparing the retention times and UV-visible spectra of the specimens with established reference standards, it was possible to swiftly identify the presence of gallic acid, epicatechin, chlorogenic acid, rosmarinic acid, caffeic acid, and apigenin. To identify the flavonoids, data relating to the flavonoid elution scheme as described in the literature were also examined in detail. Both types of rosemary steam distillation by-

product extracts contained phenolic acids and flavonoids, which have been tentatively identified in **Table 1** as two families.

According to the reference standards, peak 1,2, 3/6, 7/5, 9/7, and 10/8 for solid and water (SR/WR) residues, respectively, were positively identified as the chemical structures of gallic acid, epicatechin, chlorogenic acid, caffeic acid, rosmarinic acid, and apigenin (**Fig. 4**). The same identification was discovered by prior studies for rosemary (Bendif et al., 2017). Additionally, since the third peak's absorbance band falls within the 275–340 nm range, values that are nearly identical to the UV–vis spectra detected by numerous studies (270–340 nm), the third peak may be assumed to be homoplantaginin for the solid residue extract (Miguel Herrero et al., 2010). According to the UV-vis spectrum of peak 4 for the water residue, protocatechic acid glycoside was recognized for this peak with maxima at 220.0 and 281.2 nm, which is almost identical to the spectra given by literature data for the same plant (M. Herrero et al., 2010). For peaks 4 and 5 for solid and water residues, respectively, flavanol gallocatechin is highly recommended, whose maximum spectra were recorded between 283 and 335 nm, values quite close to those corresponding in our study (283, 334 nm). Further, the patterns of the two UV spectra are similar, demonstrating that those peaks are linked to gallocatechin (Almela et al., 2006). Based on the spectrum maximum at 275.3 nm, which is characteristic of spectral maxima observed in several studies (de Almeida Gonçalves et al., 2018) (Gonçalves et al., 2019), yunnaneic acid F is the most suggested structure for peak 8 of the water residue extract.

Comparing the two aqueous by-product extracts, the water residue remained to extract more phenolic compounds than the solid residue that could be attributed to the prolonged contact of the plant material with boiling water, a cell permeation effect favoring the extraction of the metabolites can be assumed. The harsh steam distillation conditions can also cause the

458 formation of phenolic artefacts in the water residue. In addition, high recovery of rosmarinic
459 acid and protocatechuic acid glycoside was revealed in water residue, while epicatechin and
460 homoplantagenin had to be extracted to the maximum in the solid residue. Caffeic acid is
461 extracted in almost the same way in both residues, meaning that it takes longer to extract it in
462 its entirety in the aqueous residue. These findings align with prior observations by Miljanovic´
463 et al. (Miljanović et al., 2023), indicating a higher efficacity of phenolic acid (rosmarinic,
464 syringic, and caffeic acids) and flavonoid (gallocatechin and apeginin) extraction in both by-
465 products, especially in the water residue. However, a limitation arises from the inability to
466 compare products using ethanol/water as the extraction solvent for the solid residue, hindering
467 a comprehensive analysis. Discrepancies with the findings of Luca et al. (Luca et al., 2023),
468 highlight that solid and water residues had the same elution pattern for most polar compounds,
469 while phenolic diterpenes were absent in the water residue. The authors compared the two by-
470 products with a different solvent extract, for which the solid residue was extracted using SC-
471 CO_2 extraction or even the solid residue from hydrodistillation extracted with methanol/water,
472 which is normal to have phenolic diterpenes since the solvents used can rapidly extract a range
473 of molecule polarities.
474
475 Moreover, observations from Wollinger et al. (Wollinger et al., 2016) regarding limited
476 phenolic compound presence in water residue (rosmarinic acid and traces of carnosol and
477 carnosic acid) underscore the potential impact of the distillation process duration. Conversely,
478 studies by Celano et al. (Celano et al., 2017) and de Elguea-Culebras et al. (de Elguea-Culebras
479 et al., 2023) reported the presence of all phenolic compounds, including phenolic diterpenes,
480 in water residue, emphasizing the complexity of compound extraction influenced by solvent
481 choice and extraction method. Despite these insights, a comprehensive elucidation of the
482 comparison between the two aqueous extracts from steam distillation by-products remains

elusive, warranting further investigation. Limited published data on the chemical composition of the aqueous residue from rosemary distillation, particularly for *Rosmarinus officinalis* L. and *Rosmarinus tournefortii* de Noé species, underscores the need for future research to validate these findings.

3.4. DPPH radical scavenging by elaborated nanoparticles

Antioxidants are widely acknowledged for their potential efficacy in treating and preventing various diseases. However, a notable limitation arises from the low permeability and poor water solubility of most antioxidants, leading to instability during storage and degradation in the gastrointestinal tract (Oliveira et al., 2021). Consequently, their practical utility has been restricted. To address this issue, the amalgamation of materials science and nanotechnology has played a pivotal role in reducing the generation of free radicals during nanoparticle production. These specialized nanoparticles, termed nano-antioxidants, have emerged as a solution (Dal Lago et al., 2011). In this study, the nanoparticles' capacity to mitigate the DPPH free radical was investigated. The efficacy of the prepared samples in this regard was assessed using a straightforward methodology, measuring their scavenging activity against this stable free radical.

Antioxidant capacities of elaborated materials are presented in **Fig. 5**. For comparison, the two types of *Rosmarinus tournefortii* de Noé by-products were also tested, and the results are illustrated in the same figure. As highlighted, the arrangement of the two types of by-products is the same, for which the incorporated AgNPs showed significantly higher inhibition in the case of SR/WR@AgNPs than the free by-products extracts, while the unsuccessful SR/WR@CuNPs and SR/WR@ZnNPs syntheses showed the lowest entrapment with DPPH inhibition respectively. Furthermore, upon comparing the evaluated scavenging capacities of the two by-product types, the water residue emerged as the most effective for incorporation.

Notably, the scavenging inhibition, ranging from 94.9 to 97.3%, remained consistently stable across tested concentrations. Conversely, the solid residue exhibited an escalating inhibition with increasing concentrations (ranging from 68.11 to 97.2%), as depicted in **Fig. 5**. Considering these compelling results, the observed differences in composition could indeed be attributed to the distinct chemical structures present in each by-product. In this context, the chemical profile obtained through HPLC-DAD analysis revealed a delicate equilibrium between flavonoids (46.34%) and phenolic acids (37.39%) in the solid residue. On the contrary, in the liquid residue, a striking predominance of phenolic acids (50.9% hydroxycinnamic acids and 32.97% hydroxybenzoic acids) over flavonoids (13.28%) was observed, leading to intriguing possibilities.

Comparing the two types of phenolic acids and flavonoids, Bhutto et al. (Bhutto et al., 2018) explored the correlation between the antioxidative potential of phenolic compounds and the plasmon characteristics of silver nanoparticles. The study revealed that flavonoids exhibit a strong optical response facilitated by the developed AgNPs, contrasting with phenolic acids. Within phenolic acids, hydroxycinnamic acid generally outperformed hydroxybenzoic acids, as assessed through both UV-vis bands and the corresponding molar absorptivity for these two types of phenolic acids. The same trend was found in the study performed by Scroccarello et al. (Scroccarello et al., 2021), where it was reported that AgNPs formed with the relative caffeic acid were significantly higher than gallic acid as one of the most hydroxybenzoic acids used. The nucleophilicity of the corresponding structures that react in an alkaline medium was likely responsible for the difference in the optical responses of AgNPs prepared by hydroxybenzoic and hydroxycinamic acids. The nucleophilicity of phenolics is affected by the substitution of electron-donating (-OH and OCH_3) and electron-withdrawing (-COOH and -CH=CH-COOH) groups, and this has an impact on how AgNPs respond optically.

Based on these compelling data, the highest activity of WR@AgNPs can be attributed to the remarkable influence of phenolic acids, particularly rosmarinic and caffeic acids. Their exceptional ability to swiftly and effectively neutralize free radicals significantly enhances the antioxidant properties of the nanoparticles, surpassing the collective effect of combining flavonoids and phenolic acids. These rapid and potent free radical scavenging capabilities play a pivotal role in bolstering the antioxidant efficacy of WR@AgNPs. The pivotal role of phenolic acids, particularly rosmarinic and caffeic acids, in driving the nanoparticles' robust antioxidant prowess is paramount in the battle against oxidative stress (Mohamad Sukri et al., 2023). The intricate interplay between these phenolic compounds and the nanoparticle matrix results in potent antioxidant effects, as evidenced by the remarkable 95% scavenging potential against free radicals showcased in the study of Harsha Haridas et al. (Harsha Haridas et al., 2023). Caffeic acid's renowned antioxidant properties are central to neutralizing reactive oxygen species and preventing oxidative damage within biological systems, facilitated by its controlled release encapsulated within the nanoparticles. Moreover, in model physiological media, rosmarinic acid demonstrated robust radical scavenging activity with overall rate constant values of 2.89×10^{10} and 3.86×10^{9} M^{-1} s^{-1} in water and pentyl ethanoate solvents, respectively (Vo et al., 2023). Furthermore, in an aqueous environment, rosmarinic acid exhibited an overall rate constant of 3.18×10^{8} M^{-1} s^{-1} for scavenging $HOO^{\bullet}$, a value approximately 2446 times greater than Trolox, a common antioxidant compound (Vo et al., 2023).

These results highlight the potent antioxidant efficacy of rosmarinic acid, underscoring its pivotal role in enhancing the antioxidant prowess of nanoparticles. The collaborative action between rosmarinic and caffeic acids and the nanoparticles creates a synergistic effect,

amplifying their combined antioxidant capabilities and underscoring their potential as effective therapeutic agents for combating oxidative damage and promoting cellular health. Through the donation of hydrogen atoms or electrons and the chelation of transition metal ions, these nanoparticles derived from rosmarinic and caffeic acids exhibit exceptional antioxidant prowess crucial in mitigating oxidative stress and fostering overall cellular well-being (Bouammali et al., 2023). This dominance of phenolic acids highlights their pivotal role in driving the nanoparticles' robust antioxidant prowess, making them key players in the battle against oxidative stress (Vieira et al., 2022). Interestingly, the synergy between flavonoids and phenolic acids does not consistently result in a proportional increase in antioxidant activity (Barbieri et al., 2020). In some instances, certain flavonoids may even interfere with the antioxidant mechanisms of phenolic acids, leading to a potentially less effective overall antioxidant response.

3.5. Nanoparticles effect on microbial growth

Increased mortality, morbidity, and treatment costs in developing nations are thought to be primarily caused by MDR bacterial strains and the infections they cause. Gram-positive, Gram-negative bacteria, moulds and yeast pathogens have all been linked to serious clinical and medical problems (Dakal et al., 2016). Thus, the wide-ranging and potent volatile compounds present in rosemary essential oil allow it to effectively combat a broad spectrum of microorganisms, making it a valuable and promising natural substitute for phenolic compounds in combating infections and microbial growth. Additionally, nanoparticles can enhance the antimicrobial efficacy of polar phenolic compounds, resulting in comparable or even superior effects to those of essential oils. In this proposal, the agar diffusion test was used to assess the antibacterial activity of the synthesized nanoparticles against two susceptible bacterial strains, *E. coli* and *S. aureus*, as well as the yeast *Rhodotorula glutinis* and the mould *Geotrichum sp*. **Table 2** shows the information regarding the antimicrobial potential. Regarding the two by-

583 products of *R. Tourneforti* de Noé obtained through steam distillation and used as controls, the
584 results revealed inhibition zones of 9.2 and 9 mm for *E. coli*, and 8.7 and 8.8 mm for *S. aureus*,
585 in the solid and water residues, respectively. For fungi, the inhibition zones were measured at
586 10 and 9.8 mm for *Geotrichum sp.*, and 14.3 and 15.2 mm for *Rhodotorula glutinis*, in the solid
587 and water residues, respectively.
588
589 As indicated in **Table 2**, the unsuccessful biosynthesis SR/WR@ZnNPs and SR/WR@CuNPs
590 had no effect for which could be we can highly observed that the antimicrobial activity did not
591 change significantly, for which the diameter measurements of the inhibition bacteria or fungi
592 varied weakly indicating that the phenolic compounds detected for the two by-products of *R.*
593 *Tourneforti* de Noé may not provide sufficient stabilization for the NPs formed, leading to rapid
594 agglomeration or degradation of the NPs. Adequate stabilization is essential to prevent NPs
595 from losing their antimicrobial efficacy. In contrast, the successfully biosynthesized
596 nanoparticles, SR/WR@AgNPs, demonstrated a notable increase in the inhibition zone against
597 Gram-negative *E. coli* (12 and 13.2 mm for water and solid residues, respectively) and Gram-
598 positive *S. aureus* (13.8 and 14 mm for water and solid residues, respectively). Similarly, the
599 antimicrobial activity against yeast *Rhodotorula glutinis* was significantly enhanced (16.8 and
600 17.4 mm for solid and water residues). However, no significant change in antimicrobial activity
601 was observed against the mould *Geotrichum sp.* compared to the two by-products without
602 AgNPs. Furthermore, it was observed that the two by-products, whether incorporated with Ag
603 or not, exhibited higher activity against Gram-positive bacteria compared to Gram-negative
604 bacteria. Comparing the two nanoparticles, SR@AgNPs appear to be more active than
605 WR@AgNPs against the two Gram bacteria, while the opposite is true for the yeast
606 *Rhodotorula glutinis*.
607

Upon analyzing the results from each residue matrix, a compelling equilibrium between flavonoids and phenolic acids emerged in the solid residue of *R. Tourneforti* de Noé. Intriguingly, over 80% of phenolic acids were concentrated in the water residue, unveiling a distinct distribution pattern between these two compound types within the plant. This observation hints at a potential synergistic effect, where the combined action of these compounds may yield a more potent antibacterial effect compared to using phenolic acids in isolation. Moreover, both flavonoids and phenolic acids displayed their prowess as reducing agents in the synthesis process of AgNPs, contributing to the formation of stable nanoparticles with controlled size and shape (Dakal et al., 2016). This assertion finds confirmation in the alluring allure of SR@AgNPs, boasting nanoparticles of uniform diameter at a mesmerizing 92.3 nm. On the other hand, the synthesis of WR@AgNPs graced us with a revelation of extraordinary proportions of bimodal size distribution. These findings shed light on the coexistence of two distinct particle populations, each proudly showcasing its unique size at 62.2 nm and 111.64 nm. The acquired findings align harmoniously with Lombardo et al.'s seminal work (Lombardo et al., 2016), underscoring that the synthesis of silver nanocomposites with a nonuniform size and aggregation yielded the lowest antibacterial activity against *E. coli* and *S. aureus* compared to the monodisperse counterpart. Further insight from Dal Lago et al. (Dal Lago et al., 2011) unveiled a compelling revelation smaller silver particles exhibited heightened bactericidal prowess compared to their larger counterparts, with distinct responses witnessed across diverse bacterial strains. From this wealth of data, a compelling conclusion emerges: the impact on bacterial cells extends beyond the chemical profile that can potentially modify AgNPs' surface properties. The uniformity of size and diameters of AgNPs appears to play a pivotal role in affecting bacterial response. However, a unique perspective emerges when considering the yeast *Rhodotorula glutinis*; it seems to be uniquely influenced solely by the reduction agents present.

3.6. DFT optimization

In the context of the study, the optimized structures of the targeted molecules extracted from the water and solid residues of *Rosmarinus tournefortii* de Noé, along with their interactions with AgNPs, are presented in **Fig. 6**. In every instance, the confirmation of reaching the lowest energy state was validated by the absence of any imaginary frequency. Initially, the calculation of molecular electrostatic potential (MEP) was conducted to predict the locations susceptible to electrophilic and nucleophilic reactions within the molecules under investigation. The distribution of charge in the carbohydrate molecules is predominantly influenced by the oxygen atoms due to their lone pairs. Notably, the carboxylic group within homoplantaginin exhibited the most electronegative potential, implying a strong affinity for attracting electron-deficient species. Oxygen atoms, being highly active have the ability to donate electron density to silver atoms. This suggests the plausibility of transferring an electron to a silver atom, thereby transforming an Ag^{+} cation into Ag^{0} and completing the $5s^{2}$ and $4d^{9}$ orbitals. To substantiate this concept, various Ag_{1}-complexes were constructed by altering the positioning of silver relative to the oxygen atom within the examined molecules. The silver clusters self-arranged to maximize interactions with the molecules (He and Zeng, 2010). Based on resulting energy evaluations, the most stable complexes emerged when the oxygen atom was positioned near the carboxylic group. Consequently, this same configuration was adopted for subsequent investigations.

Referring to He and Zeng's findings, the strategic placement of the silver atom and clusters was established in close proximity to the carboxyl group, a pivotal center within the carbohydrate molecules. This configuration resulted in the complexes assuming the lowest energy state. Previous investigations into reactivity patterns indicated that the primary interaction between bioactive compounds and the silver ion predominantly occurred through the carboxylic acid or

hydroxyl groups (Al-Otaibi et al., 2023). For this interaction to occur, both atoms (Ag and O) must be in contact, underscoring the significance of the distance between the silver cluster atoms and the carbohydrate molecule in comprehending these systems (Gallegos et al., 2022). Within complex formations, distances wield considerable influence and provide insights into the nature of interactions. Among the one-silver-atom complexes, the interaction energies were notably elevated, ranging from 158 to 269 kcal/mol. However, these complexes exhibited notably elongated Ag–O distances, indicating a relatively weaker interaction due to the limited number of silver atoms involved. Conversely, the Ag_3-complexes exhibited slightly lower energies (ranging from 130 to 239 kcal/mol) yet showcased shorter Ag–O distances. This indicates that complexes formed with three-silver-atom clusters are thermodynamically preferred over those involving a single silver atom. As the complexes increase in the number of silver atoms, the distances tend to approach an average length, consequently resulting in a decrease in interaction energies. The disparities in energy values and Ag–O distances are primarily governed by the specific type of carbohydrate utilized, ultimately driving improved interactions and the formation of more stabilized complexes.

Based on our investigation, a silver nanoparticle composed of 3 silver atoms is anticipated to possess superior attributes owing to its enhanced stability in contrast to smaller nanoparticles. The most stable configuration of the three-silver-atom cluster in contact with the bioactive molecule exhibits uniform bond lengths measuring 2.73 Å and is characterized by a 58.7° angle. **Fig. 7** illustrates the optimized energies of individual molecules, isolated silver atoms, and the resultant complexes. Notably, the silver cluster specifically Ag_3 interacting with the biological molecule exhibited heightened stability in comparison to either the standalone silver nanoparticle or the isolated biological molecule, as indicated by the lower energy levels. Comparing the target molecules, the complexes formed between Ag_3 and homoplantaginin,

683 protocatechuic acid-glycoside, and rosmarinic acid exhibit the most substantial interaction
684 energies, measuring 357.05, 255.33, and 266.03 kcal/mol, respectively. This indicates a
685 favourable binding between the three-silver-atom clusters and these specific molecules,
686 underpinned by the presence of electrostatic interactions (Kusumaningsih et al., 2023).
687 Significantly, these molecules also manifest the shortest Ag–O distances among all
688 compounds, averaging around 2.2-2.3 Å. Furthermore, a low bond distance of approximately
689 2.2 Å between the silver atom and the carbonyl functional group of caffeic acid was
690 demonstrated. Notably, the Ag–O distances for all four compounds (caffeic acid,
691 homoplantaginin, protocatechuic acid-glycoside, and rosmarinic acid) closely align with a
692 typical oxygen-silver bond distance of approximately 2.20-2.35 Å (Njogu et al., 2017).
693 Consequently, these molecules are anticipated to exhibit enhanced reducing activity and offer
694 a high potential for promoting the stability of AgNPs.

695 ### 3.7. Challenges and future outlook

696 An emerging beacon of hope in biomedical applications lies in the realm of green nanoparticles,
697 representing a promising alternative to conventional approaches. These nanoparticles, derived
698 from natural sources or synthesized through eco-friendly methods, offer a sustainable avenue
699 for advancing healthcare solutions. Embracing the principles of environmental consciousness,
700 green nanoparticles present a harmonious fusion of efficacy and ecological responsibility
701 (Shreyash et al., 2021). As they make their debut on the biomedical stage, their potential shines
702 through in various domains, from drug delivery to diagnostics, tissue engineering, and beyond
703 (Sher et al., 2024). These eco-conscious nanoparticles not only demonstrate biomedical
704 prowess but also carry the potential to alleviate concerns regarding the environmental impact
705 of traditional nanoparticle synthesis (Selmani et al., 2022). By embracing the synergy between
706 innovation and sustainability, green nanoparticles beckon a transformative era in biomedical
707 research and applications, where medical progress goes hand in hand with ecological

stewardship. In the context of the study, the dynamic attributes inherent to AgNPs embedded within both the solid and water residues derived from steam distillation of rosemary have been successfully demonstrated. However, an intriguing challenge arises concerning the synthesis of ZnNPs and CuNPs. Despite exhaustive analysis, including an assessment of their biological activities, successful synthesis has proven elusive. This phenomenon could potentially be ascribed to the complex interactions between the phenolic compounds and the stabilization of CuNPs and ZnNPs. While the developed nanoparticles exhibit remarkable efficiency, there are pertinent issues that demand future attention. In the subsequent sections, delving into these challenges and offering insightful perspectives for further exploration.

3.7.1. Alternative complexation agents for surface modifications

The biosynthesis of metallic nanoparticles is a multifaceted process influenced by various factors such as light exposure, plant extract composition, enzymes, metal ion concentration, and reaction conditions, collectively shaping the mechanism, synthesis rate, and final particle morphology (El-Seedi et al., 2019). This collaborative amalgamation of influences defines the bio-synthesis journey, offering the potential for process refinement and the customization of nanoparticles for specific applications. Within this realm, a harmonious interplay exists between chemical-reducing agents and the latent potential of medicinal plants. Polysaccharides like β-D-glucose and starch serve as eco-conscious reducing agents, demonstrating biocompatibility and water solubility, thus eliminating the need for hazardous solvents (Damiri et al., 2023). Various plant components, including stems, flowers, leaves, and seeds, showcase inherent reducing abilities (Alshameri and Owais, 2022). In scenarios where medicinal plants alone may not suffice for metal ion reduction, chemical-reducing agents such as $NaBH_4$ emerge as viable alternatives due to their economic viability, reproducibility, consistent particle size distribution, and straightforward experimental protocols. This strategic convergence of

732 medicinal plants' resources with the precision of chemical agents forms a synergistic approach,
733 harnessing both their inherent capabilities and the reliability of chemical-reducing agents.
734
735 Shervani et al. (Shervani and Yamamoto, 2011) conducted a comprehensive exploration into
736 the synthesis of gold (Au) nanoparticles, delving into the influence of various reducing agents,
737 encompassing both traditional chemical methods and environmentally friendly alternatives.
738 The researchers skillfully combined agents such as $NaBH_4$ and β-D-glucose, thereby refining
739 the craftsmanship of AuNPs. This holistic approach unveiled an intriguing synergy among
740 these components, orchestrating the transformation of Au salts into monodispersed AuNPs
741 characterized by a distinctive and enchanting wine-red hue a hallmark of their successful
742 formation (Shervani and Yamamoto, 2011). In their methodology, soluble starch and β-D-
743 glucose played crucial roles as carbohydrates in the synthesis process. The study highlighted
744 the successful production of monodispersed Ag(0) nanoparticles, with a diameter of 15 nm,
745 achieved by reducing $AgNO_3$ precursor salt in a starch-water gel with β-D-glucose (Shervani
746 and Yamamoto, 2011). The investigation into Au(0) metallic nanoparticles revealed the
747 nuanced impact of the reducing agent type, quantity, and solution pH on the size and
748 morphology of the nanoparticles. Notably, $NaBH_4$ at 4 equivalents produced the smallest
749 metallic particles (5.3 nm). However, an excess of $NaBH_4$ led to the nanoparticles settling out
750 as a precipitate, forming a mesh or wire structure (Shervani and Yamamoto, 2011). This
751 meticulous exploration of synthesis conditions and their effects underscores the precision
752 required in the production of metallic nanoparticles with specific size and morphology
753 characteristics.
754
755 Another noteworthy endeavour was undertaken by Bikdeloo et al. (Bikdeloo et al., 2021),
756 employing two reduction agents, $NaBH_4$ and green rosemary extract, to successfully synthesize

copper nanoparticles with a hydrodynamic diameter within the range of 50 nm. The reduction of Cu salt by $NaBH_4$ unfolded as a direct and uncomplicated process. Upon introducing $NaBH_4$ into a dispersion of rosemary extract containing the Cu precursor salt, electrons and hydrogen converged, setting the stage for the reduction of Cu salt, ultimately transforming it into lustrous metallic Cu (Bikdeloo et al., 2021). Throughout this intricate orchestration, rosemary extract played a pivotal dual role, functioning as both a reducing and stabilizing agent, underscoring the intricate harmony within this endeavour.

Delving deeper into innovation, the realm of mental association opens an alternative pathway for achieving advanced nanocomposite stabilization while harnessing the reduction capabilities of medicinal plants (Kunwar et al., 2023). The combination of metals (Cu, Zn, and Ag) introduces unique reduction reagents, creating nanocomposites with enhanced stability. This dynamic approach reinforces structural integrity by seamlessly incorporating stabilizing agents, counteracting agglomeration, and facilitating robust bonds between functional groups and metal ions. The intricate interplay of surface interactions extends to surface modifications, empowering nanocomposites with adaptability, enhanced dispersibility, amplified interactions, and heightened biocompatibility. This strategic evolution equips nanocomposites to bridge disciplinary gaps, aligning with dynamic demands (Zhang et al., 2023).

3.7.2. Multifaceted mechanisms of AgNPs toxicity and nanoparticle interactions in inflammation

Nano-silver toxicity manifests through various mechanisms at different levels, encompassing organ, cellular, and subcellular dimensions. At the organ level, nano-silver can enter the body through various exposure pathways, spreading to vital organs such as the heart, liver, kidney, brain, testes, and ovaries, thereby potentially triggering organ-specific pathophysiological effects (Zhang et al., 2022). On the cellular plane, nano silver engages with membrane proteins,

triggers signaling pathways, and disrupts cellular metabolism. Additionally, it generates reactive oxygen species (ROS), inflicts DNA damage, and upregulates autophagy, culminating in cell apoptosis (Attarilar et al., 2020). The cytotoxicity of nano silver is intricately linked to factors such as particle size, concentration, exposure duration, and the presence of stabilizers. Delving into the subcellular intricacies, nano silver exerts influences on lysosomal activity, inhibits the expression of transcription factor EB (TFEB), and disrupts the normal functioning of lysosomes. Furthermore, it interferes with ion channels on the cell membrane, creating an imbalance in cell membrane potential and leading to cell necrosis (Mehnath et al., 2021).

Shifting focus to inflammation, an immediate response to internal injury, infection, or external factors involves a nuanced interplay of immune cells and signals. Dysregulation in these signals triggers inflammation, prompting the recruitment of macrophages, killer cells, and stem cells (Fagiani et al., 2022). Macrophages, pivotal in regulating inflammation, manifest in two phenotypes: pro-inflammatory M1 and anti-inflammatory M2. During inflammation, macrophages engulf cellular debris and foster inflammation through the production of activation signals like extracellular matrix proteins, lipopolysaccharide (LPS), and cytokines. Neutrophils, in response to inflammation, migrate to the site, produce pro-inflammatory mediators, and attract macrophages (Niu et al., 2021). Upon entering the body, metal nanoparticles (NPs) encounter blood plasma proteins, resulting in the formation of a protein corona around the NP (**Fig. 8**). This corona, comprising proteins like immunoglobulin G (IgG), immunoglobulin M (IgM), and fibrinogen, crucial in the natural inflammatory process, is intricately shaped by NP properties (Bashiri et al., 2023). Serum proteins, displaying a strong attraction, play a significant role in forming the protein corona, which determines the external appearance of the NP and gives it a biological identity. This identity then governs the NP's movement and its interaction with various chemical reactions.

NPs gain entry into cells through pores or ion channels in the cell membrane, with uptake influenced by their size. Adhesive interactions, driven by electrostatic, Van der Waals, or steric forces, orchestrate the cellular uptake (Agarwal et al., 2019). The interaction between protein-coated metal NPs and macrophages or neutrophils at inflammatory sites is facilitated by the protein corona, primarily comprised of serum proteins (Cai and Chen, 2019). This protein corona acts as a ligand for receptors on anti-inflammatory M2 macrophages, triggering their activation. This activation amplifies NP uptake, with M2 macrophages exhibiting heightened and swifter NP uptake compared to M1 macrophages in the presence of serum proteins. Neutrophils, responding to stimuli, form extracellular traps (NETs), ensnaring gold nanoparticles within these NETs. This intricate mechanism underscores the pivotal role of NPs in modulating inflammatory responses and their dynamic interactions with immune cells.

3.7.3. Harnessing rosmarinic acid nanoparticles for inflammatory conditions

Inflammatory bowel disease (IBD), a complex and recurrent condition with an unknown aetiology, demands increased attention as a critical public health concern. Classified into two major subtypes, Crohn's disease (CD) and ulcerative colitis (UC), UC specifically manifests as a chronic inflammatory disorder of the rectum and colon (Kaplan and Windsor, 2021). Addressing the intricate nature of IBD, Chung et al.'s ground-breaking study explores the potential of PEGylated rosmarinic acid nanoparticles (RANPs) derived from rosemary extract as a nanomedicine for IBD treatment (Chung et al., 2020). With a diameter of 63.5 ± 4.0 nm, RANPs exhibit superior therapeutic efficacy, synergizing with conventional medication, scavenging reactive oxygen species (ROS), and protecting against oxidative damage. In a mouse model of acute colitis, RANPs treatment at doses of 20 mg/kg and 30 mg/kg significantly reduces body weight loss, bloody stools, and disease activity index (DAI) scores, indicating a substantial decrease in inflammation and damage to the colon. Histological

analysis further reveals the restoration of the colon lining structure and attenuation of inflammation (Chung et al., 2020). Additionally, RANPs dose-dependently attenuate colonic muscle thickening, supporting their role in reducing inflammation and damage to the colon. Mechanistically, RANPs inhibit the activation of pro-inflammatory transcription factors NF-κB and STAT3, and attenuate neutrophil infiltration in the inflamed colon (Chung et al., 2020). Loading the corticosteroid medication DEX into RANPs enhances therapeutic efficacy, demonstrating greater reductions in DAI scores and colon shortening compared to bare RANPs. Importantly, RANPs exhibit good biocompatibility both in vitro and in vivo, positioning them as a promising therapeutic nanomedicine for various inflammatory diseases, including IBD. This provides visual evidence of the therapeutic effects of experimental modalities on colitis-associated tissue damage and inflammation.

Relating to the broader context of inflammatory conditions, the study seamlessly aligns with investigations into rheumatoid arthritis (RA). Recognizing RA's enduring challenge to global public health, Lu et al.'s research explores antioxidative nanomedicine using ribonucleoproteins (RNPs) derived from a natural polyphenol-based compound (Lu et al., 2023). The study's schematic illustration delineates the fabrication process of RNPs (RosA nanoparticles) and reveals their therapeutic mechanism against RA. Synthesized through self-assembling oxidative oligomerization of RosA, RNPs play a crucial role in alleviating oxidative stress in RA joints, scavenging ROS, elevating the anti-inflammatory M2 subtype through macrophage polarization, and augmenting the production of anti-inflammatory cytokines (Lu et al., 2023). The RNPs exhibit the ability to inhibit synovitis, angiogenesis, cartilage degradation, and bone erosion, as evidenced by reduced clinical scores, ankle-joint thickness, and inflammation in the RNPs-treated group compared to the RosA-treated group.

The study provides insights into the cellular uptake of RNPs, emphasizing their rapid internalization within hours by cells (Lu et al., 2023). The fluorescence imaging analysis showcases the presence of RNPs in both the nuclei and cytoplasm of RAW 264.7 cells, indicating efficient cellular uptake. In vivo, biodistribution studies further underscore the excellent targeting ability of RNPs, with enhanced accumulation at inflammatory joints observed in fluorescence imaging of the paws of rats with collagen-induced arthritis (CIA). This seamless connection between studies reveals a common thread in addressing inflammatory conditions through nanomedicine, offering innovative and targeted therapeutic approaches.

4. Conclusions

The utilization of by-products generated from *Rosmarinus tournefortii* de Noé steam distillation as metal-reducing agents in the "green" synthesis of nanoparticles offers a promising route for sustainable and environmentally friendly nanomaterial production. These nanoparticles, whether sourced naturally or synthesized ecologically, exceed efficacy norms while embracing environmental responsibility. The synthesized nanoparticles underwent comprehensive characterization using UV-vis, XRD, FTIR, SEM/EDX, and Zeta analysis. The study successfully enhanced the synthesis of AgNPs using two distinct by-products, water and solid residues. However, ZnNPs and CuNPs synthesis encountered limitations, as indicated by spectroscopic characterization. Factors such as inadequate synthesis conditions, nanoparticle oxidation, agglomeration during synthesis, and the absence of appropriate surface ligands or stabilizing agents may have contributed to these challenges. The average crystallite size of AgNPs was found to be 17.98 and 18.49 nm for SR@Ag and WR@Ag composites, respectively, with stable and negative Zeta potential values (ζ values: -22.8 and -17.2 mV), suggesting nanoparticle stability. Both types of by-products yielded nanoparticles with predominantly spherical morphology, featuring varying nanoscale diameters. Antioxidant

assessment favoured water residue, showing consistent scavenging inhibition (94.9–97.3%) across concentrations, while antimicrobial activity against Gram-negative, Gram-positive bacteria, and yeast *Rhodotorula glutinis* was notably enhanced. Furthermore, DFT analysis unveiled significant interactions among homoplantaginin, rosmarinic acid, protocatechuic acid-glycoside, and caffeic acid, resulting in heightened reduction activity of AgNPs. These interactions exhibited substantial energy values, measuring 357.05, 266.03, 255.33, and 130.62 kcal/mol, respectively. These findings collectively advance the understanding of "green" nanoparticle synthesis, paving the way for further innovation and applications in diverse fields. Challenges and opportunities persist, including the pursuit of alternative complexation agents for surface modification. Shifting focus, the section explores the multifaceted toxicity mechanisms of silver nanoparticles at organ, cellular, and subcellular levels, emphasizing their intricate interactions with inflammation processes. Additionally, it introduces two promising nanomedicine approaches one involving PEGylated rosmarinic acid nanoparticles, a compound derived from rosemary extract, for treating inflammatory bowel disease, and another utilizing ribonucleoprotein for addressing rheumatoid arthritis. These findings underscore the potential of nanotechnology, particularly harnessing rosemary-derived compounds like rosmarinic acid, in innovative and targeted therapeutic interventions for diverse inflammatory conditions.

Declaration of interests

The authors declare that they have no known competing financial interests or personal relationships that could have appeared to influence the work reported in this paper.

Acknowledgements

The authors extend their genuine gratitude to Cluster Valbiom Maroc and the International Society of Engineering Science and Technology (ISEST) UK for the financial support provided. A. El Guerraf acknowledges financial support from the Czech Science Foundation

(GACR), project 22-23407S. The authors are also thank the Researchers Supporting Project number (RSP2024R169), King Saud University, Riyadh, Saudi Arabia for the financial support.

References

Abdollahzadeh, E., Nematollahi, A., Hosseini, H., 2021. Composition of antimicrobial edible films and methods for assessing their antimicrobial activity: A review. Trends Food Sci. Technol. 110, 291–303. https://doi.org/10.1016/j.tifs.2021.01.084

Adra, H.J., Lim, D., Kim, H., Jeong, K., Luo, K., Kim, Y.-R., 2024. Precision-controlled synthesis of monodisperse starch nanoparticles: Factors affecting the self-assembly kinetics. Food Hydrocoll. 110081. https://doi.org/10.1016/j.foodhyd.2024.110081

Agarwal, H., Nakara, A., Shanmugam, V.K., 2019. Anti-inflammatory mechanism of various metal and metal oxide nanoparticles synthesized using plant extracts: A review. Biomed. Pharmacother. 109, 2561–2572. https://doi.org/10.1016/j.biopha.2018.11.116

Al-Otaibi, J.S., Mary, Y Sheena, Mary, Y Shyma, Krátký, M., Vinsova, J., Gamberini, M.C., 2023. DFT, TD-DFT and SERS analysis of a bioactive benzohydrazide's adsorption in silver hydrosols at various concentrations. J. Mol. Liq. 373, 121243. https://doi.org/10.1016/j.molliq.2023.121243

Almela, L., Sánchez-Muñoz, B., Fernández-López, J.A., Roca, M.J., Rabe, V., 2006. Liquid chromatograpic-mass spectrometric analysis of phenolics and free radical scavenging activity of rosemary extract from different raw material. J. Chromatogr. A 1120, 221–229. https://doi.org/10.1016/j.chroma.2006.02.056

Alshameri, A.W., Owais, M., 2022. Antibacterial and cytotoxic potency of the plant-mediated synthesis of metallic nanoparticles Ag NPs and ZnO NPs: A Review. OpenNano. 8, 100077. https://doi.org/10.1016/j.onano.2022.100077

Attarilar, S., Yang, Jinfan, Ebrahimi, M., Wang, Q., Liu, J., Tang, Y., Yang, Junlin, 2020. The Toxicity Phenomenon and the Related Occurrence in Metal and Metal Oxide Nanoparticles: A Brief Review From the Biomedical Perspective. Front. Bioeng. Biotechnol. 8, 822. https://doi.org/10.3389/fbioe.2020.00822

935 Barbieri, J.B., Goltz, C., Cavalheiro, F.B., Toci, A.T., Igarashi-Mafra, L., Mafra, M.R., 2020.
936 Deep eutectic solvents applied in the extraction and stabilization of rosemary (Rosmarinus
937 officinalis L.) phenolic compounds. Ind. Crops Prod. 144, 112049.
938 https://doi.org/10.1016/j.indcrop.2019.112049
939 Bashiri, G., Padilla, M.S., Swingle, K.L., Shepherd, S.J., Mitchell, M.J., Wang, K., 2023.
940 Nanoparticle protein corona: from structure and function to therapeutic targeting. Lab
941 Chip. 23, 1432-1466. https://doi.org/10.1039/D2LC00799A
942 Bendif, H., Boudjeniba, M., Djamel Miara, M., Biqiku, L., Bramucci, M., Caprioli, G., Lupidi,
943 G., Quassinti, L., Sagratini, G., Vitali, L.A., Vittori, S., Maggi, F., 2017. Rosmarinus
944 eriocalyx: An alternative to Rosmarinus officinalis as a source of antioxidant compounds.
945 Food Chemistry. 218, 78-88. https://doi.org/10.1016/j.foodchem.2016.09.063
946 Bereza-Malcolm, L.T., Mann, G., Franks, A.E., 2015. Environmental sensing of heavy metals
947 through whole cell microbial biosensors: a synthetic biology approach. ACS Synth. Biol.
948 4, 535–546. https://doi.org/10.1021/sb500286r
949 Bhutto, A.A., Kalay, Ş., Sherazi, S.T.H., Culha, M., 2018. Quantitative structure–activity
950 relationship between antioxidant capacity of phenolic compounds and the plasmonic
951 properties of silver nanoparticles. Talanta 189, 174–181.
952 https://doi.org/10.1016/j.talanta.2018.06.080
953 Bikdeloo, M., Ahsani Irvani, M., Roosta, H.R., Ghanbari, D., 2021. Green synthesis of Copper
954 Nanoparticles Using Rosemary Extract to Reduce Postharvest Decays Caused by Botrytis
955 Cinerea in Tomato. J. Nanostructures 11, 834–841.
956 https://doi.org/10.22052/JNS.2021.04.020
957 Borah, R., Ninakanti, R., Nuyts, G., Peeters, H., Pedrazo-Tardajos, A., Nuti, S., Vande Velde,
958 C., De Wael, K., Lenaerts, S., Bals, S., 2021. Selectivity in the Ligand Functionalization
959 of Photocatalytic Metal Oxide Nanoparticles for Phase Transfer and Self-Assembly

Applications. Chem. Eur. J. 27, 9011–9021. https://doi.org/10.1002/chem.202100029

Bouammali, H., Zraibi, L., Ziani, I., Merzouki, M., Bourassi, L., Fraj, E., Challioui, A., Azzaoui, K., Sabbahi, R., Hammouti, B., Jodeh, S., Hassiba, M., Touzani, R., 2023. Rosemary as a Potential Source of Natural Antioxidants and Anticancer Agents: A Molecular Docking Study. Plants 13, 89. https://doi.org/10.3390/plants13010089

Cai, R., Chen, C., 2019. The crown and the scepter: roles of the protein corona in nanomedicine. Adv. Mater. 31, 1805740. https://doi.org/10.1002/adma.201805740

Celano, R., Piccinelli, A.L., Pagano, I., Roscigno, G., Campone, L., De Falco, E., Russo, M., Rastrelli, L., 2017. Oil distillation wastewaters from aromatic herbs as new natural source of antioxidant compounds. Food Res. Int. 99, 298–307. https://doi.org/10.1016/j.foodres.2017.05.036

Chen, Z., Chen, L., Khoo, K.S., Gupta, V.K., Sharma, M., Show, P.L., Yap, P.S., 2023. Exploitation of lignocellulosic-based biomass biorefinery: A critical review of renewable bioresource, sustainability and economic views. Biotechnol. Adv. 69, 108265. https://doi.org/10.1016/j.biotechadv.2023.108265

Chung, C.H., Jung, W., Keum, H., Kim, T.W., Jon, S., 2020. Nanoparticles Derived from the Natural Antioxidant Rosmarinic Acid Ameliorate Acute Inflammatory Bowel Disease. ACS Nano 14, 6887–6896. https://doi.org/10.1021/acsnano.0c01018

Da Silva, R.P.F.F., Rocha-Santos, T.A.P., Duarte, A.C., 2016. Supercritical fluid extraction of bioactive compounds. TrAC Trends Anal. Chem. 76, 40–51. https://doi.org/10.1016/j.trac.2015.11.013

Dakal, T.C., Kumar, A., Majumdar, R.S., Yadav, V., 2016. Mechanistic basis of antimicrobial actions of silver nanoparticles 7, 1831. https://doi.org/10.3389/fmicb.2016.01831

Dal Lago, V., França de Oliveira, L., de Almeida Gonçalves, K., Kobarg, J., Borba Cardoso, M., 2011. Size-selective silver nanoparticles: Future of biomedical devices with enhanced

985 bactericidal properties. J. Mater. Chem. 21, 12267–12273.
986 https://doi.org/10.1039/c1jm12297e
987 Damiri, F., Fatimi, A., Santos, A.C.P., Varma, R.S., Berrada, M., 2023. Smart stimuli-
988 responsive polysaccharide nanohydrogels for drug delivery: a review. J. Mater. Chem. B.
989 11, 10538-10565. https://doi.org/10.1039/D3TB01712E
990 Das, J., Velusamy, P., 2013. Antibacterial effects of biosynthesized silver nanoparticles using
991 aqueous leaf extract of Rosmarinus officinalis L. Mater. Res. Bull. 48, 4531–4537.
992 https://doi.org/10.1016/j.materresbull.2013.07.049
993 de Almeida Gonçalves, G., de Sa-Nakanishi, A.B., Comar, J.F., Bracht, L., Dias, M.I., Barros,
994 L., Peralta, R.M., Ferreira, I.C.F.R., Bracht, A., 2018. Water soluble compounds of
995 Rosmarinus officinalis L. improve the oxidative and inflammatory states of rats with
996 adjuvant-induced arthritis. Food Funct. 9, 2328–2340.
997 https://doi.org/10.1039/C7FO01928A
998 de Elguea-Culebras, G.O., Panamá-Tapia, L.A., Melero-Bravo, E., Cerro-Ibáñez, N., Calvo-
999 Martínez, A., Sánchez-Vioque, R., 2023. Comparison of the phenolic composition and
1000 biological capacities of wastewater from Origanum vulgare L., Rosmarinus officinalis L.,
1001 Salvia lavandulifolia Vahl. and Thymus mastichina L. resulting from two hydrodistillation
1002 systems: Clevenger and MAE. J. Appl. Res. Med. Aromat. Plants 34, 100480.
1003 https://doi.org/10.1016/j.jarmap.2023.100480
1004 de Souza Niero, A.L., Possolli, N.M., da Silva, D.F., Demétrio, K.B., Zocche, J.J., de Souza,
1005 G.M.S., Dias, J.F., Vieira, J.L., Barbosa, J.D.V., Soares, M.B.P., 2023. Composite beads
1006 of alginate and biological hydroxyapatite from poultry and mariculture for hard tissue
1007 repair. Ceram. Int. 49, 25319-25332. https://doi.org/10.1016/j.ceramint.2023.05.068
1008 El-Seedi, H.R., El-Shabasy, R.M., Khalifa, S.A.M., Saeed, A., Shah, A., Shah, R., Iftikhar,
1009 F.J., Abdel-Daim, M.M., Omri, A., Hajrahand, N.H., 2019. Metal nanoparticles fabricated

by green chemistry using natural extracts: Biosynthesis, mechanisms, and applications. RSC Adv. 9, 24539–24559. https://doi.org/10.1039/C9RA02225B

El Guerraf, A., Jadi, S. Ben, Ziani, I., Dalli, M., Sher, F., Bazzaoui, M., Bazzaoui, E.A., 2023. Multifunctional Smart Conducting Polymers-Silver Nanocomposites-Modified Biocellulose Fibers for Innovative Food Packaging Applications. Ind. Eng. Chem. Res. 62, 4540–4553. https://doi.org/10.1021/acs.iecr.2c01327

Fagiani, F., Di Marino, D., Romagnoli, A., Travelli, C., Voltan, D., Di Cesare Mannelli, L., Racchi, M., Govoni, S., Lanni, C., 2022. Molecular regulations of circadian rhythm and implications for physiology and diseases. Signal Transduct. Target. Ther. 7, 41. https://doi.org/10.1038/s41392-022-00899-y

Farshchi, H.K., Azizi, M., Jaafari, M.R., Nemati, S.H., Fotovat, A., 2018. Green synthesis of iron nanoparticles by Rosemary extract and cytotoxicity effect evaluation on cancer cell lines. Biocatal. Agric. Biotechnol. 16, 54–62. https://doi.org/10.1016/j.bcab.2018.07.017

Gallegos, F.E., Meneses, L.M., Cuesta, S.A., Santos, J.C., Arias, J., Carrillo, P., Pilaquinga, F., 2022. Computational Modeling of the Interaction of Silver Clusters with Carbohydrates. ACS Omega 7, 4750–4756. https://doi.org/10.1021/acsomega.1c04149

Ghaedi, M., Yousefinejad, M., Safarpoor, M., Khafri, H.Z., Purkait, M.K., 2015. Rosmarinus officinalis leaf extract mediated green synthesis of silver nanoparticles and investigation of its antimicrobial properties. J. Ind. Eng. Chem. 31, 167–172. https://doi.org/10.1016/j.jiec.2015.06.020

Gitipour, A., El Badawy, A., Arambewela, M., Miller, B., Scheckel, K., Elk, M., Ryu, H., Gomez-Alvarez, V., Santo Domingo, J., Thiel, S., Tolaymat, T., 2013. The Impact of Silver Nanoparticles on the Composting of Municipal Solid Waste. Environ. Sci. Technol. 47, 14385–14393. https://doi.org/10.1021/es402510a

Gonçalves, G.A., Corrêa, R.C.G., Barros, L., Dias, M.I., Calhelha, R.C., Correa, V.G., Bracht,

A., Peralta, R.M., Ferreira, I.C.F.R., 2019. Effects of in vitro gastrointestinal digestion and colonic fermentation on a rosemary (Rosmarinus officinalis L) extract rich in rosmarinic acid. Food Chem. 271, 393–400. https://doi.org/10.1016/j.foodchem.2018.07.132

Harsha Haridas, E.S., Bhattacharya, S., Varma, M.K.R., Chandra, G.K., 2023. Bioinspired 5-caffeoylquinic acid capped silver nanoparticles using Coffee arabica leaf extract for high-sensitive cysteine detection. Sci. Rep. 13, 1–12. https://doi.org/10.1038/s41598-023-34944-9

He, Y., Zeng, T., 2010. First-principles study and model of dielectric functions of silver nanoparticles. J. Phys. Chem. C 114, 18023–18030. https://doi.org/10.1021/jp101598j

Herrero, Miguel, Plaza, M., Cifuentes, A., Ibáñez, E., 2010. Green processes for the extraction of bioactives from Rosemary: Chemical and functional characterization via ultra-performance liquid chromatography-tandem mass spectrometry and in-vitro assays. J. Chromatogr. A 1217, 2512–2520. https://doi.org/10.1016/j.chroma.2009.11.032

Herrero, M., Plaza, M., Cifuentes, A., Ibáñez, E., 2010. Green processes for the extraction of bioactives from Rosemary: Chemical and functional characterization via ultra-performance liquid chromatography-tandem mass spectrometry and in-vitro assays. J. Chromatogr. A 1217, 2512–2520. https://doi.org/10.1016/j.chroma.2009.11.032

Huh, A.J., Kwon, Y.J., 2011. “Nanoantibiotics”: a new paradigm for treating infectious diseases using nanomaterials in the antibiotics resistant era. J. Control. release 156, 128–145.

Jahan, I., Erci, F., Isildak, I., 2021. Facile microwave-mediated green synthesis of non-toxic copper nanoparticles using Citrus sinensis aqueous fruit extract and their antibacterial potentials. J. Drug Deliv. Sci. Technol. 61, 102172. https://doi.org/10.1016/j.jddst.2020.102172

1060 Jędrzejczyk, R.J., Gustab, M., Ważny, R., Domka, A., Jodłowski, P.J., Sitarz, M., Bezkosty,
1061 P., Kowalski, M., Pawcenis, D., Jarosz, K., 2023. Iron inactivation by Sporobolomyces
1062 ruberrimus and its potential role in plant metal stress protection. An in vitro study. Sci.
1063 Total Environ. 870, 161887. https://doi.org/10.1016/j.scitotenv.2023.161887
1064 Kaplan, G.G., Windsor, J.W., 2021. The four epidemiological stages in the global evolution of
1065 inflammatory bowel disease. Nat. Rev. Gastroenterol. Hepatol. 18, 56–66.
1066 https://doi.org/10.1038/s41575-020-00360-x
1067 Kaushik, V., Kagdada, H.L., Singh, D.K., Pathak, S., 2022. Enhancement of SERS effect in
1068 Graphene-Silver hybrids. Appl. Surf. Sci. 574, 151724.
1069 https://doi.org/10.1016/j.apsusc.2021.151724
1070 Kelly, K.L., Coronado, E., Zhao, L.L., Schatz, G.C., 2003. The optical properties of metal
1071 nanoparticles: the influence of size, shape, and dielectric environment. J. Phys. Chem. B.
1072 107, 3, 668–677. https://doi.org/10.1021/jp026731y
1073 Kim, D.-Y., Yang, T., Srivastava, P., Nile, S.H., Seth, C.S., Jadhav, U., Syed, A., Bahkali,
1074 A.H., Ghodake, G.S., 2024. Alginic acid-functionalized silver nanoparticles: A rapid
1075 monitoring tool for detecting the technology-critical element tellurium. J. Hazard. Mater.
1076 465, 133161. https://doi.org/10.1016/j.jhazmat.2023.133161
1077 Kim, Y., Ji, S., Nam, J.-M., 2023. A Chemist's View on Electronic and Steric Effects of Surface
1078 Ligands on Plasmonic Metal Nanostructures. Acc. Chem. Res. 56, 2139–2150.
1079 https://doi.org/10.1021/acs.accounts.3c00196
1080 Kotakadi, V.S., Gaddam, S.A., Rao, Y.S., Prasad, T., Reddy, A.V., Gopal, D.V.R.S., 2014.
1081 Biofabrication of silver nanoparticles using Andrographis paniculata. Eur. J. Med. Chem.
1082 73, 135–140. https://doi.org/10.1016/j.ejmech.2013.12.004
1083 Kunwar, S., Roy, A., Bhusal, U., Gacem, A., Abdullah, M.M.S., Sharma, P., Yadav, K.K.,
1084 Rustagi, S., Chatterjee, N., Deshwal, V.K., 2023. Bio-Fabrication of Cu/Ag/Zn

1085 Nanoparticles and Their Antioxidant and Dye Degradation Activities. Catalysts 13, 891.
1086 https://doi.org/10.3390/catal13050891
1087 Kusumaningsih, T., Prasetyo, W.E., Istiqomah, A., Firdaus, M., Wibowo, F.R., 2023.
1088 Sustainable synthesis of silver nanoparticles with enhanced anticancer, antibacterial, and
1089 antioxidant properties mediated by dimeric 2,4-diacetyl phloroglucinol: Experimental and
1090 computational insights. Surfaces and Interfaces 36, 102545.
1091 https://doi.org/10.1016/j.surfin.2022.102545
1092 Lee, J., Chae, K.-J., 2021. A systematic protocol of microplastics analysis from their
1093 identification to quantification in water environment: A comprehensive review. J. Hazard.
1094 Mater. 403, 124049. https://doi.org/10.1016/j.jhazmat.2020.124049
1095 Liu, T., Sui, X., Zhang, R., Yang, L., Zu, Y., Zhang, L., Zhang, Y., Zhang, Z., 2011.
1096 Application of ionic liquids based microwave-assisted simultaneous extraction of carnosic
1097 acid, rosmarinic acid and essential oil from Rosmarinus officinalis. J. Chromatogr. A
1098 1218, 8480–8489. https://doi.org/10.1016/j.chroma.2011.09.073
1099 Lombardo, P.C., Poli, A.L., Castro, L.F., Perussi, J.R., Schmitt, C.C., 2016. Photochemical
1100 Deposition of Silver Nanoparticles on Clays and Exploring Their Antibacterial Activity.
1101 ACS Appl. Mater. Interfaces 8, 21640–21647. https://doi.org/10.1021/acsami.6b05292
1102 Lu, B., Li, C., Jing, L., Zhuang, F., Xiang, H., Chen, Y., Huang, B., 2023. Rosmarinic acid
1103 nanomedicine for rheumatoid arthritis therapy: Targeted RONS scavenging and
1104 macrophage repolarization. J. Control. Release 362, 631–646.
1105 https://doi.org/10.1016/j.jconrel.2023.09.012
1106 Luca, S.V., Zengin, G., Sinan, K.I., Korona-Glowniak, I., Minceva, M., Skalicka-Woźniak, K.,
1107 Trifan, A., 2023. Value-Added Compounds with Antimicrobial, Antioxidant, and
1108 Enzyme-Inhibitory Effects from Post-Distillation and Post-Supercritical CO2 Extraction
1109 By-Products of Rosemary. Antioxidants. 12, 244.

https://doi.org/10.3390/antiox12020244

Lv, Z., He, S., Wang, Y., Zhu, X., 2021. Noble metal nanomaterials for NIR-triggered photothermal therapy in cancer. Adv. Healthc. Mater. 10, 2001806. https://doi.org/10.1002/adhm.202001806

Mahdi, M.A., Yousefi, S.R., Jasim, L.S., Salavati-Niasari, M., 2022. Green synthesis of DyBa2Fe3O7. 988/DyFeO3 nanocomposites using almond extract with dual eco-friendly applications: photocatalytic and antibacterial activities. Int. J. Hydrogen Energy 47, 14319–14330. https://doi.org/10.1016/j.ijhydene.2022.02.175

Martins, T.A.G., Falconi, I.B.A., Pavoski, G., de Moraes, V.T., Galluzzi Baltazar, M. dos P., Espinosa, D.C.R., 2021. Green synthesis, characterization, and application of copper nanoparticles obtained from printed circuit boards to degrade mining surfactant by Fenton process. J. Environ. Chem. Eng. 9, 106576. https://doi.org/10.1016/j.jece.2021.106576

Mehnath, S., Das, A.K., Verma, S.K., Jeyaraj, M., 2021. Biosynthesized/green-synthesized nanomaterials as potential vehicles for delivery of antibiotics/drugs, 1st ed, Comprehensive Analytical Chemistry. Elsevier. 94, 363-432. https://doi.org/10.1016/bs.coac.2020.12.011

Miljanović, A., Dent, M., Grbin, D., Pedisić, S., Zorić, Z., Marijanović, Z., Jerković, I., Bielen, A., 2023. Sage, Rosemary, and Bay Laurel Hydrodistillation By-Products as a Source of Bioactive Compounds. Plants. 12 (13), 2394. https://doi.org/10.3390/plants12132394

Mittal, A.K., Chisti, Y., Banerjee, U.C., 2013. Synthesis of metallic nanoparticles using plant extracts. Biotechnol. Adv. 31, 346–356. https://doi.org/10.1016/j.biotechadv.2013.01.003

Mohamad Sukri, S.N.A., Shameli, K., Teow, S.Y., Chew, J., Ooi, L.T., Lee-Kiun Soon, M., Ismail, N.A., Moeini, H., 2023. Enhanced antibacterial and anticancer activities of plant extract mediated green synthesized zinc oxide-silver nanoparticles. Front. Microbiol. 14, 1–14. https://doi.org/10.3389/fmicb.2023.1194292

1135 Naghdi, M., Ghovvati, M., Rabiee, N., Ahmadi, S., Abbariki, N., Sojdeh, S., Ojaghi, A.,
1136 Bagherzadeh, M., Akhavan, O., Sharifi, E., 2022. Magnetic nanostructures in
1137 nanomedicine revolution: A review of growing magnetic nanocomposites in biomedical
1138 applications. Adv. Colloid Interface Sci. 308, 102771.
1139 https://doi.org/10.1016/j.cis.2022.102771
1140 Niu, Y., Wang, Z., Shi, Y., Dong, L., Wang, C., 2021. Modulating macrophage activities to
1141 promote endogenous bone regeneration: Biological mechanisms and engineering
1142 approaches. Bioact. Mater. 6, 244–261. https://doi.org/10.1016/j.bioactmat.2020.08.012
1143 Njogu, E.M., Omondi, B., Nyamori, V.O., 2017. Coordination polymers and discrete
1144 complexes of Ag (I)-N-(pyridylmethylene) anilines: Synthesis, crystal structures and
1145 photophysical properties. J. Coord. Chem. 70, 2796–2814.
1146 https://doi.org/10.1080/00958972.2017.1370088
1147 Noukelag, S.K., Razanamahandry, L.C., Ntwampe, S.K.O., Arendse, C.J., Maaza, M., 2021.
1148 Industrial dye removal using bio-synthesized Ag-doped ZnO nanoparticles. Environ.
1149 Nanotechnology, Monit. Manag. 16, 100463.
1150 https://doi.org/10.1016/j.enmm.2021.100463
1151 Oliveira, A.L.S., Gondim, S., Gómez-García, R., Ribeiro, T., Pintado, M., 2021. Olive leaf
1152 phenolic extract from two Portuguese cultivars –bioactivities for potential food and
1153 cosmetic application. J. Environ. Chem. Eng. 9, 106175.
1154 https://doi.org/10.1016/j.jece.2021.106175
1155 Piñeros-Hernandez, D., Medina-Jaramillo, C., López-Córdoba, A., Goyanes, S., 2017. Edible
1156 cassava starch films carrying rosemary antioxidant extracts for potential use as active food
1157 packaging. Food Hydrocoll. 63, 488–495. https://doi.org/10.1016/j.foodhyd.2016.09.034
1158 Pisoschi, A.M., Iordache, F., Stanca, L., Gajaila, I., Ghimpeteanu, O.M., Geicu, O.I., Bilteanu,
1159 L., Serban, A.I., 2022. Antioxidant, anti-inflammatory, and immunomodulatory roles of

1160 nonvitamin antioxidants in anti-SARS-CoV-2 therapy. J. Med. Chem. 65, 12562–12593.
1161 https://doi.org/10.1021/acs.jmedchem.2c01134
1162 Pryshchepa, O., Pomastowski, P., Buszewski, B., 2020. Silver nanoparticles: Synthesis,
1163 investigation techniques, and properties. Adv. Colloid Interface Sci. 284, 102246.
1164 https://doi.org/10.1016/j.cis.2020.102246
1165 Rabiee, N., Bagherzadeh, M., Kiani, M., Ghadiri, A.M., 2020. Rosmarinus officinalis directed
1166 palladium nanoparticle synthesis: Investigation of potential anti-bacterial, anti-fungal and
1167 Mizoroki-Heck catalytic activities. Adv. Powder Technol. 31, 1402–1411.
1168 https://doi.org/10.1016/j.apt.2020.01.024
1169 Rambabu, K., Bharath, G., Banat, F., Show, P.L., 2021. Green synthesis of zinc oxide
1170 nanoparticles using Phoenix dactylifera waste as bioreductant for effective dye
1171 degradation and antibacterial performance in wastewater treatment. J. Hazard. Mater. 402,
1172 123560. https://doi.org/10.1016/j.jhazmat.2020.123560
1173 Rao, B.R., Kumar, R., Haque, S., Kumar, J.M., Rao, T.N., Kothapalli, R.V.S.N., Patra, C.R.,
1174 2021. Ag2 [fe (cn) 5no]-fabricated hydrophobic cotton as a potential wound healing
1175 dressing: An in vivo approach. ACS Appl. Mater. Interfaces 13, 10689–10704.
1176 https://doi.org/10.1021/acsami.0c19904
1177 Raut, R.W., Mendhulkar, V.D., Kashid, S.B., 2014. Photosensitized synthesis of silver
1178 nanoparticles using Withania somnifera leaf powder and silver nitrate. J. Photochem.
1179 Photobiol. B Biol. 132, 45–55. https://doi.org/10.1016/j.jphotobiol.2014.02.001
1180 Sankaran, R., Markandan, K., Khoo, K.S., Cheng, C.K., Ashokkumar, V., Deepanraj, B., Show,
1181 P.L., 2021. The Expansion of Lignocellulose Biomass Conversion Into Bioenergy via
1182 Nanobiotechnology. Front. Nanotechnol. 3, 1–10.
1183 https://doi.org/10.3389/fnano.2021.793528
1184 Scroccarello, A., Junior, B.M.-H., Della Pelle, F., Ciancetta, J., Ferraro, G., Fratini, E.,

Valbonetti, L., Copez, C.C., Compagnone, D., 2021. Effect of phenolic compounds-capped AgNPs on growth inhibition of Aspergillus niger. Colloids Surfaces B Biointerfaces 199, 111533. https://doi.org/10.1016/j.colsurfb.2020.111533

Selmani, A., Kovačević, D., Bohinc, K., 2022. Nanoparticles: From synthesis to applications and beyond. Adv. Colloid Interface Sci. 303, 102640. https://doi.org/10.1016/j.cis.2022.102640

Sher, F., Ziani, I., Smith, M., Chugreeva, G., Hashimzada, S.Z., Prola, L.D.T., Sulejmanović, J., Sher, E.K., 2024. Carbon quantum dots conjugated with metal hybrid nanoparticles as advanced electrocatalyst for energy applications–A review. Coord. Chem. Rev. 500, 215499. https://doi.org/10.1016/j.ccr.2023.215499

Shervani, Z., Yamamoto, Y., 2011. Carbohydrate-directed synthesis of silver and gold nanoparticles: effect of the structure of carbohydrates and reducing agents on the size and morphology of the composites. Carbohydr. Res. 346, 651–658. https://doi.org/10.1016/j.carres.2011.01.020

Shreyash, N., Bajpai, S., Khan, M.A., Vijay, Y., Tiwary, S.K., Sonker, M., 2021. Green synthesis of nanoparticles and their biomedical applications: a review. ACS Appl. Nano Mater. 4, 11428–11457. https://doi.org/10.1021/acsanm.1c02946

Tariq, G.H., Asghar, G., Shifa, M.S., Anis-Ur-Rehman, M., Ullah, S., Shah, Z.A., Ziani, I., Tawfeek, A.M., Sher, F., 2023. Effect of copper doping on plasmonic nanofilms for high performance photovoltaic energy applications. Phys. Chem. Chem. Phys. 25, 31726–31740. https://doi.org/10.1039/d3cp04332k

Usmani, Z., Sharma, Minaxi, Gaffey, J., Sharma, Monika, Dewhurst, R.J., Moreau, B., Newbold, J., Clark, W., Thakur, V.K., Gupta, V.K., 2022. Valorization of dairy waste and by-products through microbial bioprocesses. Bioresour. Technol. 346, 126444. https://doi.org/10.1016/j.biortech.2021.126444

1210 Vieira, I.R.S., de Carvalho, A.P.A. de, Conte-Junior, C.A., 2022. Recent advances in biobased
1211 and biodegradable polymer nanocomposites, nanoparticles, and natural antioxidants for
1212 antibacterial and antioxidant food packaging applications. Compr. Rev. Food Sci. Food
1213 Saf. 21, 3673–3716. https://doi.org/10.1111/1541-4337.12990
1214 Vo, Q. V., Hoa, N.T., Flavel, M., Thong, N.M., Boulebd, H., Nam, P.C., Quang, D.T., Mechler,
1215 A., 2023. A Comprehensive Study of the Radical Scavenging Activity of Rosmarinic
1216 Acid. J. Org. Chem. 88, 17237–17248. https://doi.org/10.1021/acs.joc.3c02093
1217 Wollinger, A., Perrin, É., Chahboun, J., Jeannot, V., Touraud, D., Kunz, W., 2016. Antioxidant
1218 activity of hydro distillation water residues from Rosmarinus officinalis L. leaves
1219 determined by DPPH assays. Comptes Rendus Chim. 19, 754–765.
1220 https://doi.org/10.1016/j.crci.2015.12.014
1221 Yaraki, M.T., Zahed Nasab, S., Zare, I., Dahri, M., Moein Sadeghi, M., Koohi, M., Tan, Y.N.,
1222 2022. Biomimetic metallic nanostructures for biomedical applications, catalysis, and
1223 beyond. Ind. Eng. Chem. Res. 61, 7547–7593. https://doi.org/10.1021/acs.iecr.2c00285
1224 Zhang, H., Du, W., Peralta-Videa, J.R., Gardea-Torresdey, J.L., White, J.C., Keller, A., Guo,
1225 H., Ji, R., Zhao, L., 2018. Metabolomics Reveals How Cucumber (Cucumis sativus)
1226 Reprograms Metabolites To Cope with Silver Ions and Silver Nanoparticle-Induced
1227 Oxidative Stress. Environ. Sci. Technol. 52, 8016–8026.
1228 https://doi.org/10.1021/acs.est.8b02440
1229 Zhang, J., Wang, F., Yalamarty, S.S.K., Filipczak, N., Jin, Y., Li, X., 2022. Nano Silver-
1230 Induced Toxicity and Associated Mechanisms. Int. J. Nanomedicine 17, 1851–1864.
1231 https://doi.org/10.2147/IJN.S355131
1232 Zhang, L., Zhang, M., Mujumdar, A.S., Yu, D., Wang, H., 2023. Potential nano bacteriostatic
1233 agents to be used in meat-based foods processing and storage: A critical review. Trends
1234 Food Sci. Technol. 131, 77–90. https://doi.org/10.1016/j.tifs.2022.11.023

1235 Ziani, I., Bouakline, H., Yahyaoui, M.I., Belbachir, Y., Fauconnier, M.L., Asehraou, A.,
1236 Tahani, A., Talhaoui, A., El Bachiri, A., 2023. The effect of ethanol/water concentration
1237 on phenolic composition, antioxidant, and antimicrobial activities of Rosmarinus
1238 tournefortii de Noé hydrodistillation solid residues. J. Food Meas. Charact. 17, 1602–
1239 1615. https://doi.org/10.1007/s11694-022-01722-6

1240

1241

1242

List of Tables

Table 1. Identification of phenolic compounds from *Rosmarinus tournefortii* de Noé responsible for metal ion reduction.

Peak number	Retention time (min)		Tentative identified compounds		Relative abundance (% of total peak area)	
	Water residue	Solid residue	Water residue	Solid residue	Solid residue	Water residue
1	2.13	3.41	Gallic acid	Gallic acid	9.65	0.92
2	2.66	3.92	Epicatechin	Epicatechin	17.22	7.82
3	3.03	4.39	Chlorogenic acid	Homoplantaginin	15.52	4.94
4	3.27	5.63	Protocatechuic acid- glycoside	Gallocatechin	12.24	32.05
5	3.66	5.80	Gallocatechin	Caffeic acid	31.02	4.25
6	3.99	7.84	N. I	Chlorogenic acid	2.56	2.79
7	4.43	7.95	Caffeic acid	Rosmarinic acid	3.81	23.51
8	6.08	8.80	Yunnaneic acid F	Apigenin	1.68	1.33
9	6.52	-	Rosmarinic acid	-	-	21.15
10	9.32	-	Apigenin	-	-	1.21

1247 **Table 2.** Inhibition Zones of the biosynthesized nanoparticles using *Rosmarinus tournefortii*
1248 de Noé solid and water residues.
1249

Samples	**Inhibition zone diameter (mm)**			
	E.coli	***S. aureus***	***Geotrichum sp.***	***Rhodotorula glutinis***
WR	9±0.78	8.8±0.67	9.8±0.53	15.2±0.45
WR@ZnNPs	8.9±0.35	8.7±0.95	10±0.33	16.1±0.23
WR@CuNPs	9±0.11	9.5±0.22	9.6±0.22	13±0.25
WR@AgNPs	12±0.49	13.8±0.25	10±0.63	16.8±0.56
SR	9.2±0.13	8.7±0.46	10±0.33	14.3±0.13
SR@ZnNPs	9.6±0.21	8.8±0.47	9±0.7	14.7±0.31
SR@CuNPs	8.9±0.22	9±0.88	10.2±0.22	15.2±0.12
SR@AgNPs	13.2±0.63	14±0.98	9.8±0.25	17.4± 1.02

1250

1251

List of Figures

Fig. 1. The elaboration process of silver nanoparticles using *Rosmarinus tournefortii* de Noé by-products.

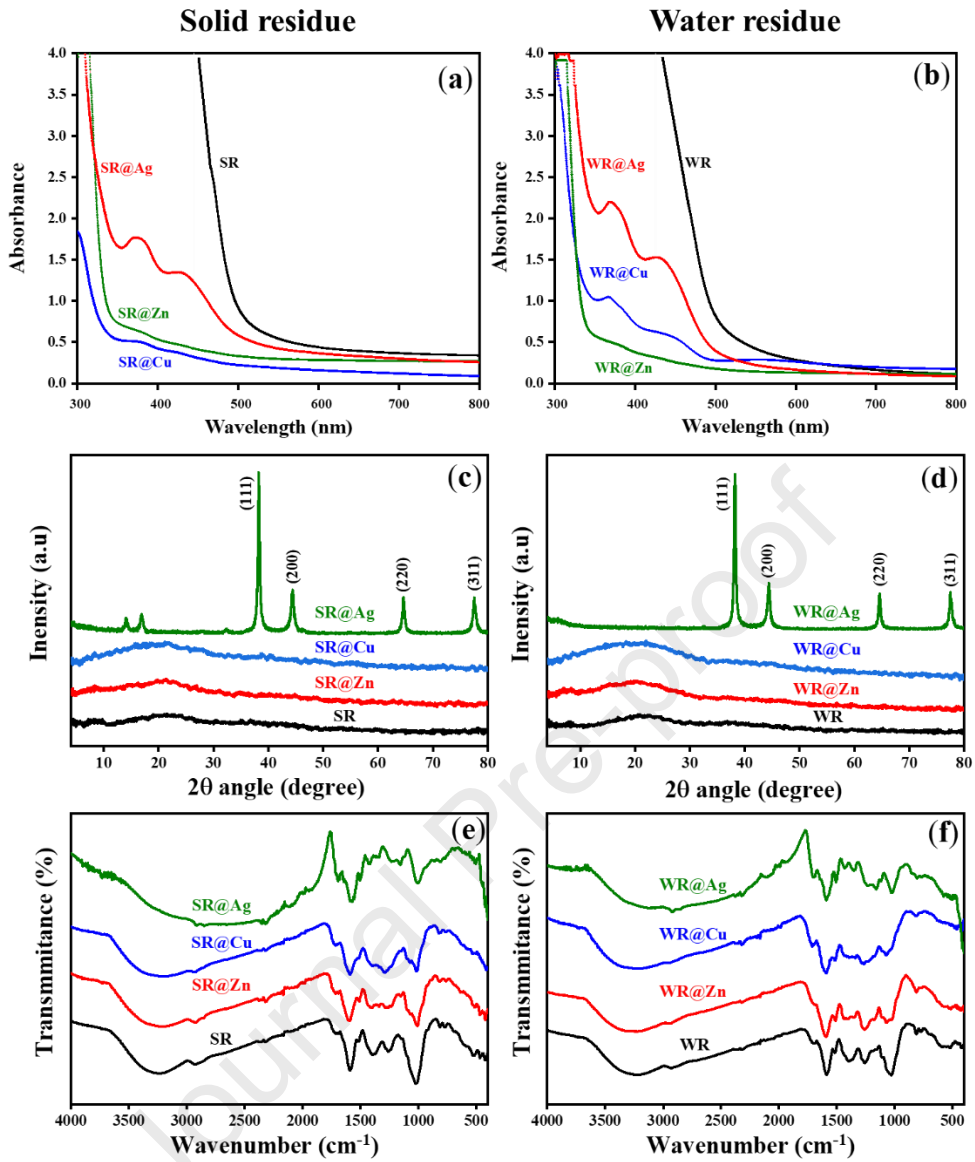

1260

1261 **Fig. 2.** (a, b) UV-visible patterns, (c, d) X-ray diffraction patterns and (e, f) FTIR profiles of

1262 biosynthesized nanoparticles using *Rosmarinus tournefortii* de Noé solid and water residues.

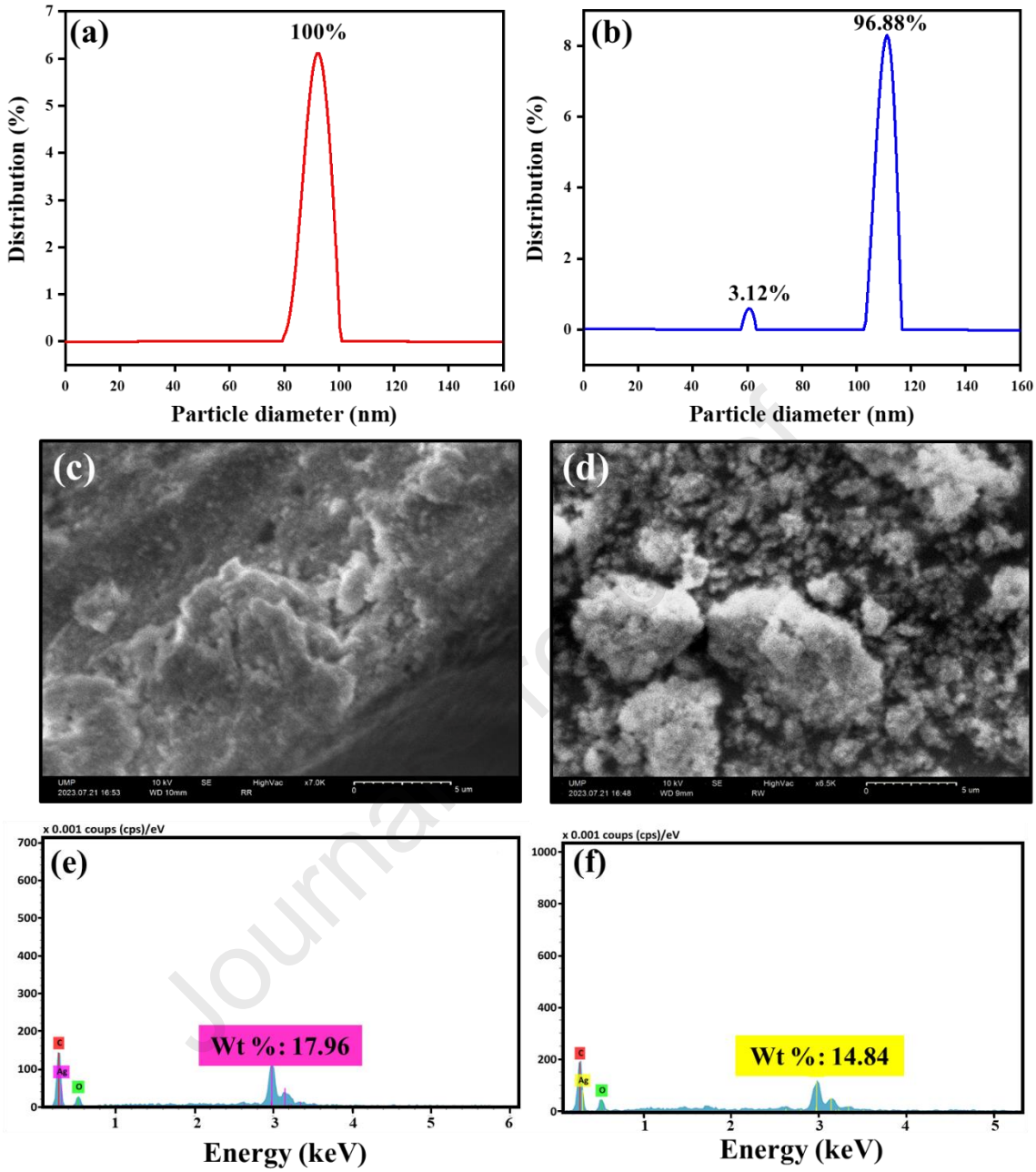

1263

1264 **Fig. 3.** Hydrodynamic size**,** SEM images and corresponding EDS spectra of synthesized AgNPs

1265 using *Rosmarinus tournefortii* de Noé; (a, c, e) solid and (b, d, f) water residues.

1266

1267

1268

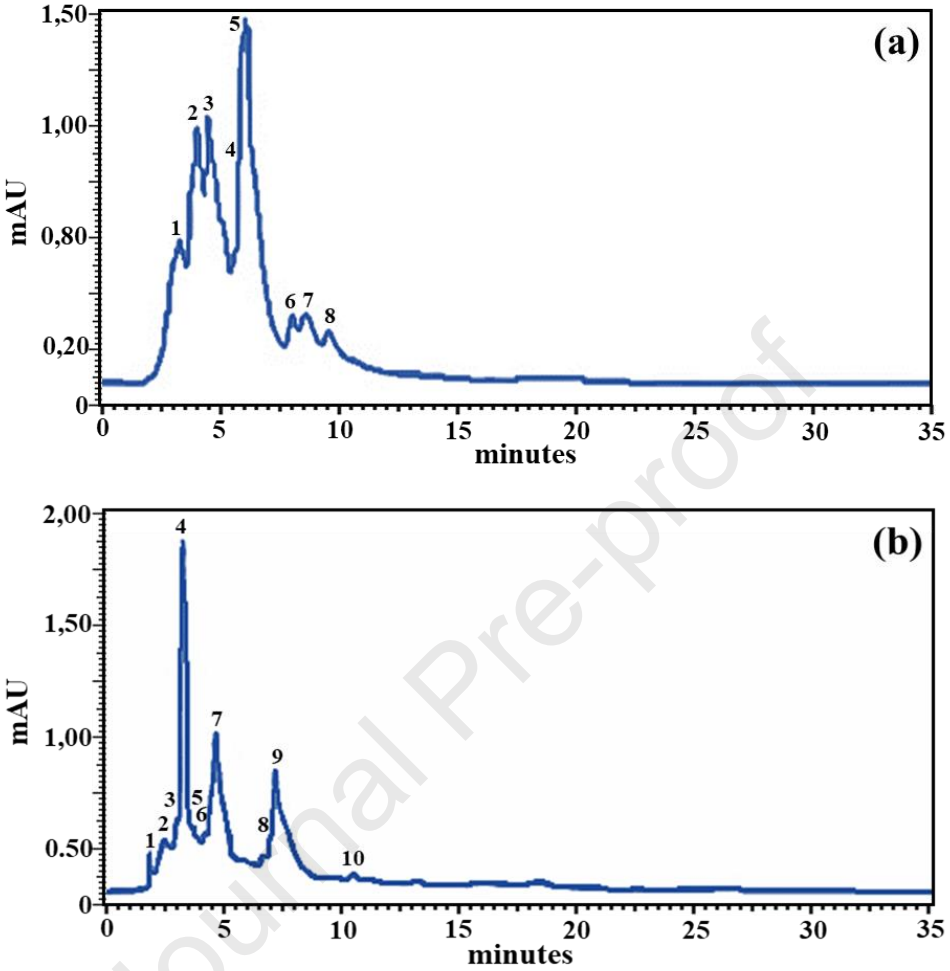

1269

1270

1271 **Fig. 4.** HPLC-DAD chromatograms of (a) the solid and (b) liquid by-products of *Rosmarinus*

1272 *tournefortii* de Noé.

1273

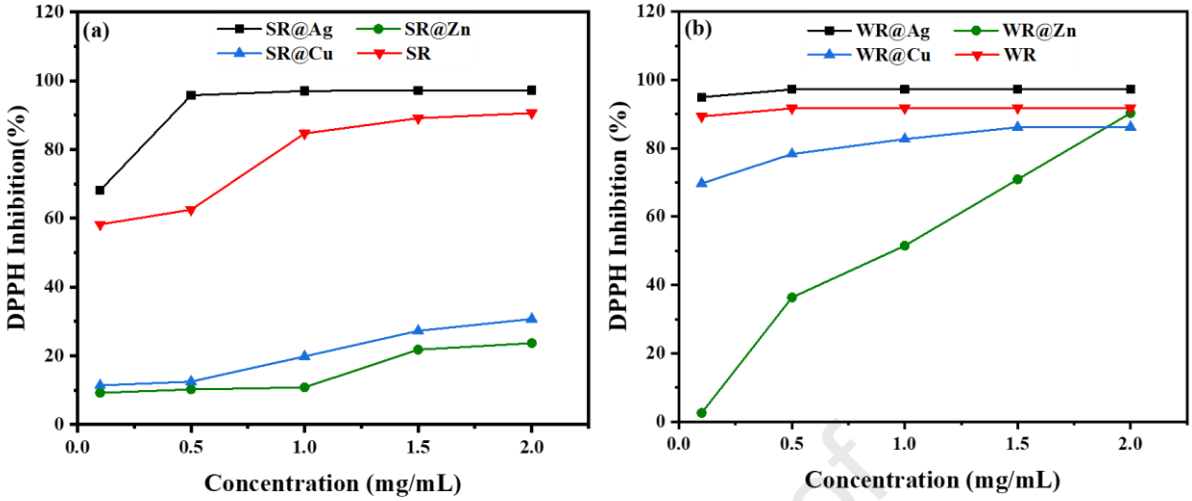

1274

1275 **Fig. 5.** Antioxidant performance of (a) the solid and (b) the water by-products and their coating
1276 with Ag, Cu and Zn.

1277

1278

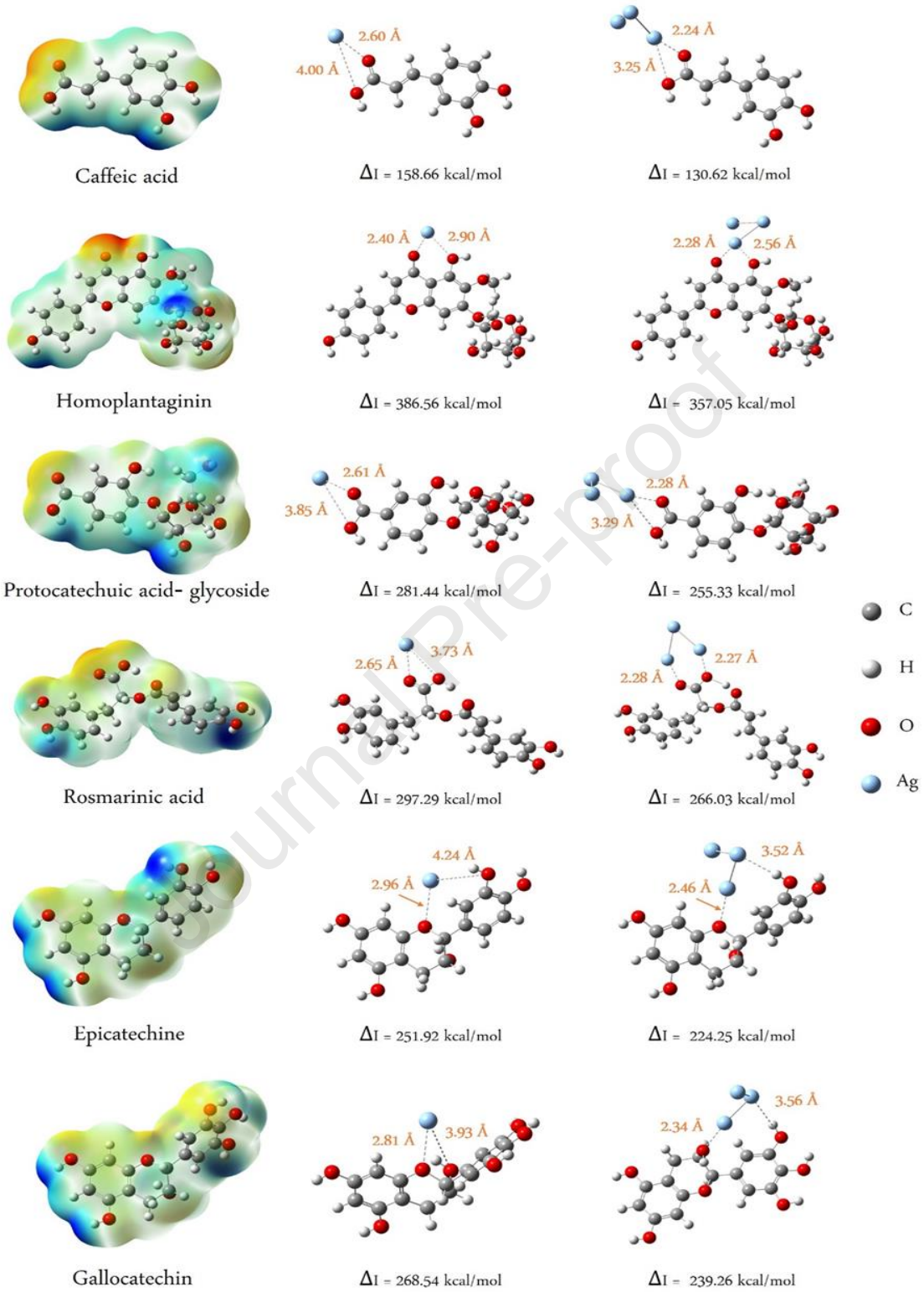

1279

1280 **Fig. 6.** Optimized geometries with the molecular electrostatic potential maps of the selected
1281 compounds with and without the inclusion of silver clusters. The interaction energies of the
1282 target molecules with Ag_1 or Ag_3 are included.

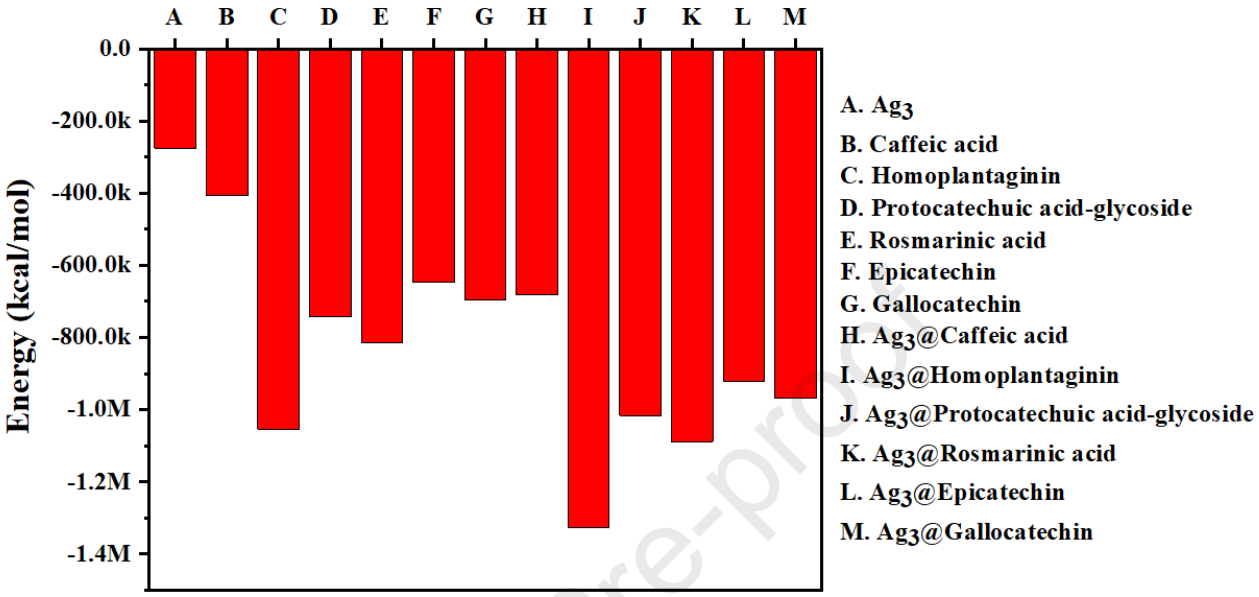

Fig. 7. Total energies of the selected compounds with and without the inclusion of silver clusters.

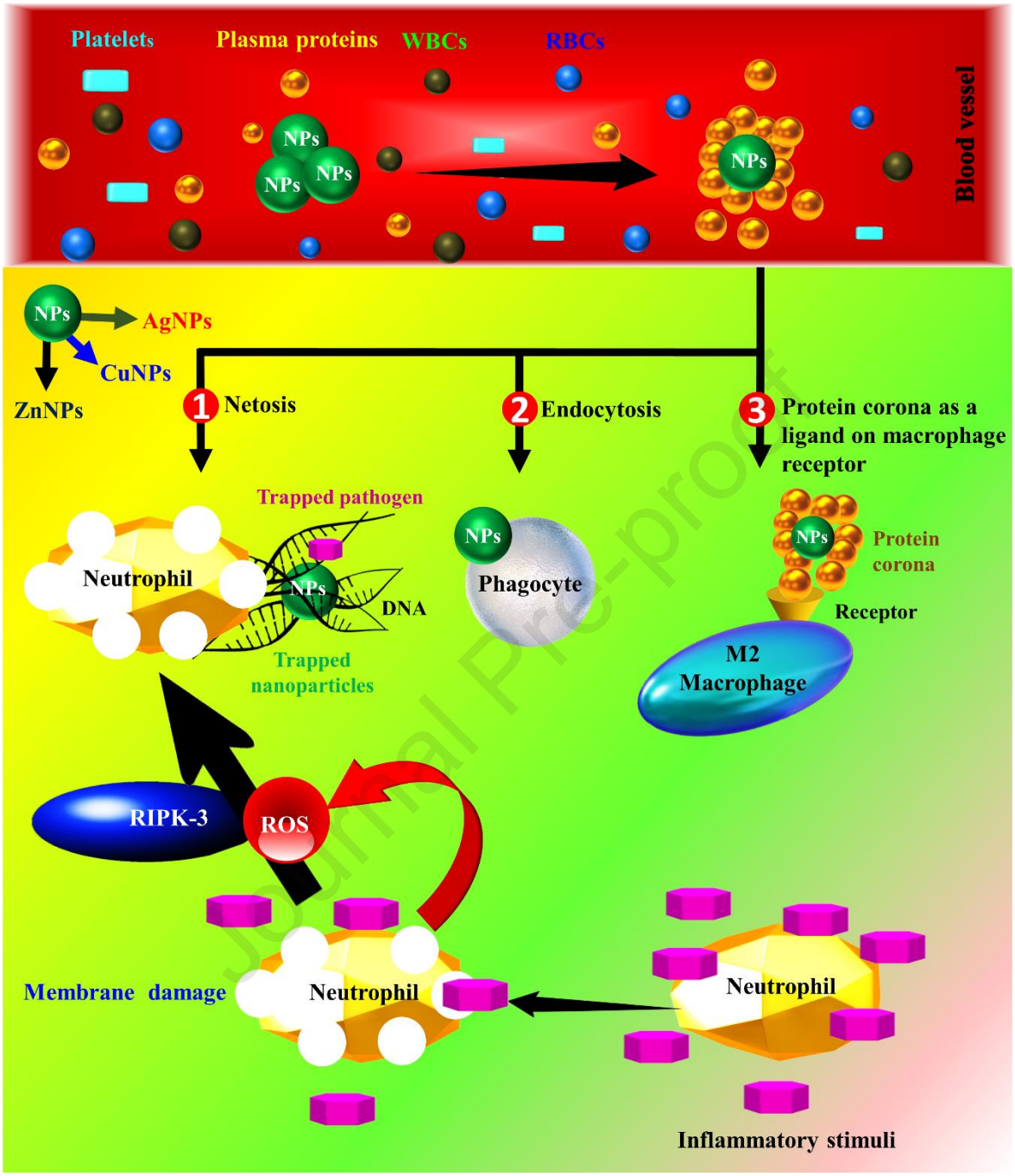

Fig. 8. Different nanoparticles employ anti-inflammatory mechanisms.

1308 # Graphical Abstract

1309

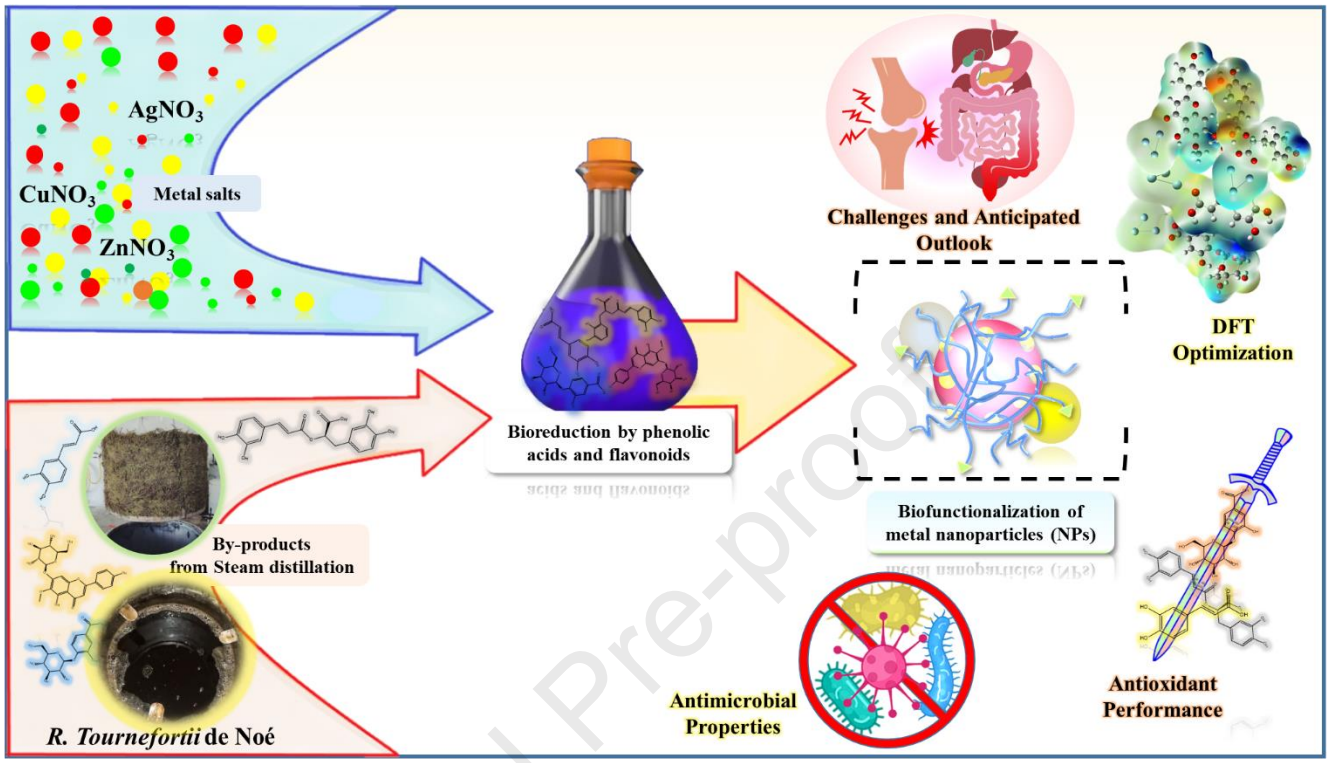

1310

Highlights

- Synergistic AgNPs synthesis using eco-friendly R. *tournefortii* de Noé by-products.
- By-products yielded spherical nanoparticles with varied nanoscale diameters.
- Enhanced antioxidant and antibacterial activities were demonstrated.
- DFT highlighted biomolecules (130.62–357.05 kcal/mol) enhancing stability.
- AgNPs toxicity mechanisms and interactions in inflammation elucidated.

Declaration of interests

☒ The authors declare that they have no known competing financial interests or personal relationships that could have appeared to influence the work reported in this paper.

☐The authors declare the following financial interests/personal relationships which may be considered as potential competing interests: